

# RADIATIVE CORRECTIONS TO A SUPERSYMMETRIC RELATION: A NEW APPROACH

Shingo Kiyoura,<sup>a,b</sup> Mihoko M. Nojiri,<sup>c</sup> Damien M. Pierce,<sup>d</sup> and Youichi Yamada<sup>e</sup>

<sup>a</sup> *KEK Theory Group, Oho 1-1, Tsukuba, Ibaraki 305-0801, Japan*

<sup>b</sup> *Department of Physics, Tokyo Institute of Technology, Oh-okayama, Meguro, Tokyo 152-8551, Japan*

<sup>c</sup> *YITP, Kyoto University, Kyoto 606-8502, Japan*

<sup>d</sup> *Stanford Linear Accelerator Center, Stanford University, Stanford, California 94309, USA*

<sup>e</sup> *Department of Physics, Tohoku University, Sendai 980-8578, Japan*

## Abstract

Recently it has been realized that the production and decay processes of charginos, neutralinos, and sleptons receive corrections which grow like  $\log m_{\tilde{q}}$  for large  $m_{\tilde{q}}$ . In this paper we calculate the chargino pair production cross section at  $e^+e^-$  colliders with quark/squark loop corrections. We introduce a novel formulation, where the one-loop amplitude is reorganized into two parts. One part is expressed in terms of the “effective” chargino coupling  $\bar{g}_{e\tilde{\nu}\tilde{W}}$  and mixing matrices  $U^P$ ,  $V^P$ , and includes all  $\mathcal{O}(\log m_{\tilde{q}})$  corrections, while the other decouples for large  $m_{\tilde{q}}$ . The form of the one-loop cross section then becomes physically transparent. Our formulation can be easily extended to other loops and processes. Numerically, we find significant corrections due to the effective  $t$ -channel coupling  $\bar{g}_{e\tilde{\nu}\tilde{W}}$ , for gaugino-like charginos. In the mixed region, where the chargino has large gaugino and Higgsino components, the corrections due to  $(U^P, V^P)$  are also significant. Our numerical results disagree with a previous calculation. We revisit previous studies of the determination of  $\bar{g}_{e\tilde{\nu}\tilde{W}}$  through the measurement of the chargino production cross section. We point out that a previous study, which claimed that the measurement suffers large systematic errors, was performed at a “pessimistic” point in MSSM parameter space. We provide reasons why the systematic errors are not a limiting factor for generic parameter choices.

# 1 Introduction

Calculations of higher loop effects in the Standard Model (SM), together with the recent precision measurements of electroweak parameters, have given rise to a wealth of information on physics at the weak scale and above. Among these measurements, one of the interesting observations is the approximate agreement of the measured gauge couplings with the prediction of supersymmetric Grand Unified Theories (GUTs) [1]. This may be regarded as indirect evidence for the minimal supersymmetric standard model (MSSM), which is the low energy effective theory of supersymmetric GUTs. Additionally, global fits to precision data in the SM prefer a light Higgs boson mass [2], which is consistent with the MSSM which predicts  $m_h \lesssim 130$  GeV.

In the near future, the Large Hadron Collider (LHC) will explore the TeV energy region. Squarks and gluinos will be discovered, together with charginos and neutralinos, if the supersymmetry breaking scale is below a few TeV. Recent studies show that certain superpartner mass differences can be measured quite precisely at the LHC [3, 4]. Furthermore, if any of the proposed lepton colliders are constructed many of MSSM parameters (e.g. the gaugino masses, the Higgsino mass  $\mu$ , the slepton masses, and the ratio of vacuum expectation values  $\tan\beta$ ) will be measured to  $\mathcal{O}(1\%) \sim \mathcal{O}(10\%)$  [5, 6, 7, 8].

The future precision measurements of new particle masses, event rates, and branching ratios, will provide for detailed tests of the supersymmetry hypothesis. Supersymmetry imposes hard relations between gaugino couplings and gauge couplings, and between Higgsino and Higgs couplings. The cancellation of Higgs mass quadratic divergences cannot be realized without these supersymmetry coupling relations. Therefore, they comprise an essential ingredient of the model. Measurements of the coupling relations will provide definitive evidence of the realization of supersymmetry in nature.

Because supersymmetry is broken, the hard coupling relations receive radiative corrections [8, 9, 10, 11, 12, 13]. Since all split supersymmetry multiplets contribute to the splitting of the gauge/gaugino and Higgs/Higgsino couplings, measurements of the splitting may provide useful information about the supersymmetry spectrum. This is readily understood from the point of view of effective field theory. As an example, below the squark mass scale the gauge and gaugino couplings run differently because squarks do not contribute to the running of the gauge or gaugino couplings, but quarks continue to contribute to the running of the gauge couplings. At a scale  $Q$  below the squark mass scale, this mismatch in the running manifests as a difference between the couplings proportional to  $\ln(m_{\tilde{q}}/Q)$  [9]. Such a correction also appears in the off-diagonal elements of the chargino and neutralino mass matrices, which originate from Higgsino-Higgs-gaugino couplings. Notice the analogy to the radiative corrections in the SM. The SM gauge symmetry relates various SM observables. Since the particle masses in the SM break the gauge symmetry, the measurement of electroweak observables leads to constraints on the particle masses, in particular the top quark and Higgs boson masses.

Corrections to supersymmetric relations were first calculated in Ref. [9] in the effective renormalization group equation (RGE) approach. For degenerate squarks, one finds the correction to lepton-slepton-gaugino couplings

$$\bar{g}_{e\tilde{\nu}\tilde{W}}/g_2^{\text{SM}} = 1 + 2\% \log_{10}(m_{\tilde{q}}/m_{\tilde{l}}) \quad (1)$$

$$\bar{g}_{e\tilde{e}\tilde{B}}/g_Y^{\text{SM}} = 1 + 0.7\% \log_{10}(m_{\tilde{q}}/m_{\tilde{l}}) . \quad (2)$$

The fermion-sfermion-gaugino couplings are involved in both the production and decay processes of charginos, neutralinos and sfermions. Studying these processes provides for measurements of the gaugino couplings. It is particularly interesting to measure the gaugino coupling at future  $e^+e^-$  colliders, because precise measurements of the differential cross section are possible there. Studies show the gauge/gaugino coupling difference may be measured within 0.3%  $\sim$  20% through the measurement of the production cross sections of sleptons or charginos [8, 11, 13]. Typically, the high sensitivity of  $\mathcal{O}(1\%)$  or less may be achieved when the collider experiments can measure both the final state superpartner masses and the mass of the particle exchanged in  $t$ -channel. Such a high precision measurement of the difference between the gauge and gaugino couplings allows for the possibility of constraining the mass scale of squarks which might not be in direct reach in either hadron or lepton collider experiments.

Because the corrections to the supersymmetric relations are large enough to be measured in proposed future experiments, it is important to calculate the full one-loop amplitude in detail. Tree level amplitudes depend on the definition of the tree level parameters. In the  $\overline{\text{DR}}$  scheme [14] the gauge couplings and chargino and neutralino mixing matrices depend on the renormalization scale. Changing the scale by a factor of 2 easily results a few percent change in the predicted value of the production cross section, about the size of the correction of interest. Such scale dependence can be curtailed only by including radiative corrections.

In this paper we present the full one-loop calculation of the chargino production cross section  $\sigma(e^-e^+ \rightarrow \tilde{\chi}_i^- \tilde{\chi}_j^+)$  including quark and squark loop contributions. The calculation has been performed previously in the  $\overline{\text{DR}}$  scheme in Ref. [15]. In their formula the mixing matrix of the chargino is scale dependent. This scale dependence must be compensated for by the chargino wave function renormalization, leading to very complicated expressions. We simplify the calculation by introducing the effective mixing matrices  $U^P, V^P$ . Expressed in terms of  $U^P, V^P$ , the formulae are reorganized into a compact and physically transparent form. This reorganization allows us to see that the full amplitude consists of two renormalization scale independent parts. One contains all the process independent corrections. For sufficiently heavy squarks, this reduces to the effective tree level amplitude which depends on process independent effective parameters. These effective parameters contain all the corrections proportional to  $\log m_{\tilde{q}}$ . The other part of the amplitude contains the process dependent contributions, i.e. the one particle irreducible (1PI) chargino vertex correction and chargino wave function renormalization. This part decouples in the large  $m_{\tilde{q}}$  limit.

In this paper, we also examine previous studies of the measurement of the effective gaugino coupling  $\bar{g}_{e\tilde{\nu}\tilde{W}}$  through the study of chargino production and decay [11], which is based on Monte Carlo (MC) study of Ref. [7]. In the study, the constraint on  $\bar{g}_{e\tilde{\nu}\tilde{W}}$  is claimed to be limited by the systematic error due to the uncertainty of the underlying parameters. The maximal sensitivity to  $\bar{g}_{e\tilde{\nu}\tilde{W}}$  obtained in Ref. [7] is 2%, which is merely enough to constrain squark mass within a factor of 10. One may ask whether a full one-loop calculation is necessary if this is always the case. However, we find the case studied in Ref. [7] is uncharacteristically pessimistic in the sense that the signature of chargino events is very similar to that of backgrounds, and this naturally makes precision measurement very difficult. We provide reasons why systematic errors are not a limiting

factor in the precision study of the supersymmetric relation.

The paper is organized as follows. In Sec. 2 we describe our formalism which reorganizes the one-loop chargino pair production amplitude, making for a more physically transparent and computationally manageable formula. In Sec. 3 we show our numerical results. The formulas presented in Sec. 2 systematically guide the discussion of the  $\log m_{\tilde{q}}$  corrections and the remaining finite corrections. In addition to corrections to the amplitude from the well studied  $\log m_{\tilde{q}}$  behavior of  $\bar{g}_{e\tilde{\nu}\tilde{W}}$ , we find the  $\log m_{\tilde{q}}$  corrections and some finite corrections to the effective mixing matrices are important when the chargino is a sizable mixture of Higgsino and gaugino. We also note in Sec. 3 that the calculation of the cross section including only top-stop and bottom-sbottom loops presented in Ref. [15] is not a reasonable approximation in general. Our numerical results disagree with the results of Ref. [15]. We discuss the validity of various approximations to the one-loop cross section. In Sec. 4 we revisit the previous study of the  $\bar{g}_{e\tilde{\nu}\tilde{W}}$  measurement from the chargino production cross section. In Ref. [11] they argue that the sensitivity to the cross section is limited due to a strong dependence of the chargino acceptance on the theoretical underlying parameters. However, this study is carried out at a point in the supersymmetry parameter space with very special kinematics. Unlike the generic supersymmetric signature, the signal has a soft  $\not{p}_T$  distribution similar to the  $WW$  background. This results in the small acceptance and the strong sensitivity to the masses under the standard set of cuts. We point out that at a generic point in parameter space the acceptance error is not large and the systematic error is not a limiting factor in the measurement. We also discuss general ways to minimize the acceptance error. Sec. 5 is saved for discussion and conclusions.

## 2 One-loop correction to chargino pair production

### 2.1 Amplitude and cross section

We show the form of the amplitudes of the chargino pair production  $e^-(p_1)e^+(p_2) \rightarrow \tilde{\chi}_i^-(p_3)\tilde{\chi}_j^+(p_4)$  including quark and squark loop corrections. We start with the tree level amplitude. The  $s$ -channel amplitude comes from the exchange of gauge bosons ( $\gamma, Z$ ). The  $t$ -channel amplitude involves the exchange of the electron sneutrino  $\tilde{\nu} \equiv \tilde{\nu}_e$ . Their sum gives

$$\begin{aligned}
i\mathcal{M}_{ij} &= i(\mathcal{M}_{ij}^{(s)} + \mathcal{M}_{ij}^{(t)}) \\
&= +ie^2 \frac{1}{s} [\bar{u}(p_3)\gamma^\mu \delta_{ij} v(p_4)] [\bar{v}(p_2)\gamma_\mu u(p_1)] \\
&\quad + ig_Z \frac{1}{s - M_Z^2} [\bar{u}(p_3)\gamma^\mu (v_{Lij}^Z P_L + v_{Rij}^Z P_R) v(p_4)] [\bar{v}(p_2)\gamma_\mu (I_{3e} P_L - s_W^2 Q_e) u(p_1)] \\
&\quad + \frac{ig_2^2}{2} \frac{V_{i1}^* V_{j1}}{t - m_{\tilde{\nu}}^2} [\bar{u}(p_3)\gamma^\mu P_R v(p_4)] [\bar{v}(p_2)\gamma_\mu P_L u(p_1)] .
\end{aligned} \tag{3}$$

where  $s = (p_1 + p_2)^2$ ,  $t = (p_1 - p_3)^2$ ,  $g_Z = g_2/c_W$ ,  $s_W = \sqrt{1 - c_W^2} = \sin \theta_W$ , and  $P_{R,L} = (1 \pm \gamma_5)/2$ . The  $u$  and  $v$  are the wave functions of  $e^\pm$  and  $\tilde{\chi}^\pm$ . We have applied a Fierz transformation to the  $t$ -channel amplitude to make its spinor structure similar to  $s$ -channel one. The  $v_{ij}^Z$  are the tree level couplings of the charginos to the  $Z$  boson, which depend on the chargino mixing matrices ( $U, V$ ). Their definitions are given in Appendix A.

We next show the form of the corrected amplitude. The loop corrections include the 1PI chargino/gauge vertex correction, the chargino wave function renormalization, and the gauge boson self energy corrections. We adopt the  $\overline{\text{DR}}$  renormalization scheme for gauge couplings and the weak mixing angle ( $e, g_2, g_Z, s_W$ ) and chargino mixing matrices ( $U, V$ ), and we adopt the on-shell scheme for the  $Z$  and  $\tilde{\nu}$  masses. Since we only include the quark and squark loop corrections, the running of the  $\overline{\text{DR}}$  parameters includes only the contributions of quarks and squarks for consistency. Note that ( $U, V$ ) are obtained by diagonalizing the tree level mass matrix Eq. (A.2) in the  $\overline{\text{DR}}$  scheme, so they are renormalization scale dependent.

The  $t$ -channel amplitude receives only chargino wave function renormalization. The corrected amplitude takes the following form

$$i\mathcal{M}_{ij}^{(t)} = \frac{ig_2^2}{2} \frac{1}{t - m_{\tilde{\nu}}^2} [\bar{u}(p_3)\gamma^\mu P_R v(p_4)] [\bar{v}(p_2)\gamma_\mu P_L u(p_1)] \\ \times (V_{i1}^* V_{j1} + \frac{1}{2}(V_{i1}^* V_{j'1} \delta Z_{j'j}^R + \delta Z_{ii'}^{R\dagger} V_{i'1}^* V_{j1})) , \quad (4)$$

where  $\delta Z^{L(R)}$  are the wave function renormalization of charginos  $\tilde{\chi}_{L(R)}^-$ . Their explicit forms are given later. Strictly speaking, the squark loop correction also appears in the sneutrino propagator. However, this momentum independent contribution is completely canceled by the on-shell renormalization of  $m_{\tilde{\nu}}^2$ .

The  $s$ -channel amplitude is corrected by oblique gauge boson propagator corrections, chargino wave function renormalization, and the 1PI chargino-chargino-gauge boson vertex correction. The form of the corrected amplitude is

$$i\mathcal{M}_{ij}^{(s)} = -ieQ_e \frac{1}{s} \left( 1 - \frac{\Pi_{\gamma\gamma}^T(s)}{s} \right) [\bar{u}(p_3)\Gamma_{ij}^{\gamma\mu} v(p_4)] [\bar{v}(p_2)\gamma_\mu u(p_1)] \\ -ie \frac{\Pi_{\gamma Z}^T(s)}{s(s - M_Z^2)} \left\{ Q_{\tilde{\chi}^-} \delta_{ij} [\bar{u}(p_3)\gamma^\mu v(p_4)] [\bar{v}(p_2)\gamma_\mu g_Z (I_{3e} P_L - s_W^2 Q_e) u(p_1)] \right. \\ \left. + Q_e [\bar{u}(p_3)\gamma^\mu (v_{Lij}^Z P_L + v_{Rij}^Z P_R) v(p_4)] [\bar{v}(p_2)\gamma_\mu u(p_1)] \right\} \\ -ig_Z \frac{1}{s - M_Z^2} \left( 1 - \frac{\Pi_{ZZ}^T(s) - \Pi_{ZZ}^T(M_Z^2)}{s - M_Z^2} \right) \\ \times [\bar{u}(p_3)\Gamma_{ij}^{Z\mu} v(p_4)] [\bar{v}(p_2)\gamma_\mu (I_{3e} P_L - s_W^2 Q_e) u(p_1)] , \quad (5)$$

where  $M_Z$  is the  $Z$ -boson pole mass. The  $\Pi^T(p^2)$  are the transverse parts of the  $\overline{\text{DR}}$  renormalized gauge-boson self-energies. Their explicit forms are given in Ref. [16, 17]. The form factors  $i\Gamma_{ij}^{G\mu}$  for one-loop corrected  $\tilde{\chi}_i^+ \tilde{\chi}_j^- G^\mu$  vertices ( $G = \gamma, Z$ ) have the following forms

$$\Gamma_{ij}^{G\mu} = -\gamma^\mu (v_{Lij}^G P_L + v_{Rij}^G P_R) \\ + F_{VL}^G \gamma^\mu P_L + F_{VR}^G \gamma^\mu P_R + F_{SL}^G (p_3 - p_4)^\mu P_L + F_{SR}^G (p_3 - p_4)^\mu P_R \\ - \frac{1}{2} (v_{Lij}^G \delta Z_{j'j}^L + \delta Z_{ii'}^{L\dagger} v_{L'j}^G) \gamma^\mu P_L - \frac{1}{2} (v_{Rij}^G \delta Z_{j'j}^R + \delta Z_{ii'}^{R\dagger} v_{R'j}^G) \gamma^\mu P_R . \quad (6)$$

The first line of Eq. (6) contains the tree level couplings (A.7) with ( $e, g_Z, U, V$ ) in the  $\overline{\text{DR}}$  scheme.  $F_V^G$  and  $F_S^G$  are the one-particle-irreducible (1PI) corrections to the vertices. Their explicit forms are given in the Appendix B. The last line gives the chargino wave function renormalization.

The wave function corrections  $\delta Z^{L,R}$  are determined in terms of the two-point function  $iK_{ij}(p)$  of charginos  $\tilde{\chi}_i^+(-p)\tilde{\chi}_j^-(p)$  in the  $\overline{\text{DR}}$  mass basis.  $K_{ij}$  is decomposed as

$$K_{ij}(p) = \Sigma_{ij}^L(p^2)\not{p}P_L + \Sigma_{ij}^R(p^2)\not{p}P_R + \Sigma_{ij}^D(p^2)P_L + \Sigma_{ji}^{D*}(p^2)P_R, \quad (7)$$

and  $\delta Z$  are then fixed by imposing well-known on-shell renormalization conditions for fermions [18]. The diagonal parts of  $\delta Z$  are

$$\begin{aligned} \delta Z_{ii}^L &= -\Sigma_{ii}^L(m_i^2) + \frac{1}{m_i} \left[ \Sigma_{ii}^D(m_i^2) - \Sigma_{ii}^{D*}(m_i^2) \right] \\ &\quad - m_i^2 \left[ \Sigma_{ii}^{L'}(m_i^2) + \Sigma_{ii}^{R'}(m_i^2) \right] - m_i \left[ \Sigma_{ii}^{D'}(m_i^2) + \Sigma_{ii}^{D'*}(m_i^2) \right] \\ \delta Z_{ii}^R &= -\Sigma_{ii}^R(m_i^2) - m_i^2 \left[ \Sigma_{ii}^{L'}(m_i^2) + \Sigma_{ii}^{R'}(m_i^2) \right] - m_i \left[ \Sigma_{ii}^{D'}(m_i^2) + \Sigma_{ii}^{D'*}(m_i^2) \right]. \end{aligned} \quad (8)$$

Here  $\Sigma'(p^2) = \partial\Sigma(p^2)/\partial p^2$ . The abbreviation  $m_i = m_{\tilde{\chi}_i^-}$  is used for convenience. The term proportional to  $\text{Im}\Sigma_{ii}^D$  in  $\delta Z_{ii}^L$  comes from our convention to use real  $\delta Z_{ii}^R$ . In this paper we treat only cases where  $\Sigma_{ii}^D(m_i^2)$  is real (no CP violation). The off-diagonal terms ( $i \neq j$ ) are

$$\begin{aligned} \delta Z_{ij}^L &= \frac{2}{m_i^2 - m_j^2} \left[ m_j^2 \Sigma_{ij}^L(m_j^2) + m_i m_j \Sigma_{ij}^R(m_j^2) + m_i \Sigma_{ij}^D(m_j^2) + m_j \Sigma_{ji}^{D*}(m_j^2) \right], \\ \delta Z_{ij}^R &= \frac{2}{m_i^2 - m_j^2} \left[ m_i m_j \Sigma_{ij}^L(m_j^2) + m_j^2 \Sigma_{ij}^R(m_j^2) + m_j \Sigma_{ij}^D(m_j^2) + m_i \Sigma_{ji}^{D*}(m_j^2) \right]. \end{aligned} \quad (9)$$

In addition, the pole masses of charginos are given by

$$m_i(\text{pole}) = m_i - \frac{1}{2} m_i \left[ \Sigma_{ii}^L(m_i^2) + \Sigma_{ii}^R(m_i^2) \right] - \frac{1}{2} \left[ \Sigma_{ii}^D(m_i^2) + \Sigma_{ii}^{D*}(m_i^2) \right]. \quad (10)$$

In the corrected amplitude Eqs. (4, 5), the renormalization scale dependence of the  $\overline{\text{DR}}$  tree level parameters and that of the loop functions exactly cancel to  $\mathcal{O}(\alpha)$ . However, the cancellation is quite complicated as we will see in the next subsection.

In the numerical calculation we take the pole masses of gauge bosons ( $Z, W$ ), and the standard model  $\overline{\text{MS}}$  electromagnetic coupling  $\alpha_{\text{SM}}(M_Z)$  as inputs. The  $\overline{\text{DR}}$  gauge couplings are obtained from these parameters as discussed in Ref. [13]. The chargino sector is fixed by giving pole masses of two charginos and  $\tan\beta(M_Z)$ .

Finally, the spin-averaged differential cross section is written in terms of the amplitude as

$$\frac{d\sigma}{d\cos\theta} = \frac{1}{2s} \frac{\bar{\beta}_{\tilde{\chi}}}{16\pi} \overline{\sum} |\mathcal{M}|^2. \quad (11)$$

Here  $\overline{\sum}$  denotes average over the initial electron and positron helicities and sum over the final chargino helicities. We use the helicity amplitude method [19] in the numerical calculation of the cross section. The relevant formulae are given in Appendix C. The phase space factor  $\bar{\beta}_{\tilde{\chi}}$  is given by

$$\bar{\beta}_{\tilde{\chi}} = \frac{1}{s} \sqrt{s^2 - 2(m_{\tilde{\chi}_i^-}^2 + m_{\tilde{\chi}_j^+}^2)s + (m_{\tilde{\chi}_i^-}^2 - m_{\tilde{\chi}_j^+}^2)^2}. \quad (12)$$

Since a highly polarized electron beam will be available at future  $e^+e^-$  linear colliders, in this paper we often present the cross section for an initial electron in a helicity eigenstate. Note that the chargino masses in  $\bar{\beta}_{\tilde{\chi}}$  and in the wave functions ( $u(p_3), v(p_4)$ ) are the pole masses.

## 2.2 On-shell Renormalization of charginos

The wave function renormalizations of charginos  $\delta Z_{ij}^{L(R)}$  appear in the corrected amplitude Eqs. (4, 5). They contain ultraviolet divergences from  $(\Sigma^L, \Sigma^R, \Sigma^D)$  and, after  $\overline{\text{DR}}$  renormalization, depend on the renormalization scale  $Q$ . This  $Q$  dependence cancels the implicit  $Q$  dependence of the  $\overline{\text{DR}}$  mixing matrices  $(U, V)$ , the gauge coupling  $g_2$  in Eq. (4), and the explicit dependence of the 1PI vertex corrections in Eq. (6). However, this cancellation is quite complicated. For example, in Eq. (6) the  $Q$  dependence of the off-diagonal parts of  $\delta Z^L$  cancels both that of  $U$  in  $v_L^G$  and that of  $F_{VL}^G$ . Moreover, the off-diagonal parts of  $\delta Z^{L(R)}$  in Eq. (9) superficially diverge when two chargino masses become degenerate. Therefore the forms of  $\delta Z^{L(R)}$  in Eqs. (4, 5) can be inconvenient in real calculations.

In this subsection, we reorganize the contribution of  $\delta Z^{L(R)}$  into a very convenient form, by utilizing the  $Q$ -independent effective chargino mixing matrices  $(U^P, V^P)$ . The loop contributions which compensate the running of  $(U, V)$  are then completely split from other corrections.

We first notice that both the diagonal and off-diagonal parts of the chargino wave function renormalization  $\delta Z^{L(R)}$  can be implemented by making the following replacements in the couplings of the tree level amplitude,

$$\begin{aligned} U_{ik}^\dagger &\rightarrow U_{ik}^\dagger + \frac{1}{2} U_{ij}^\dagger \delta Z_{jk}^L, \\ V_{ik}^T &\rightarrow V_{ik}^T + \frac{1}{2} V_{ij}^T \delta Z_{jk}^R. \end{aligned} \quad (13)$$

The corrections Eq. (13) are universal in any processes involving on-shell charginos. Remember that in Eq. (13) the mixing matrices  $(U, V)$  diagonalize the  $\overline{\text{DR}}$  tree level mass matrix Eq. (A.2).

The factors in Eq. (13) come from the relations between the  $\overline{\text{DR}}$  fields in the gauge eigenbasis  $\psi_i^-$ , the  $\overline{\text{DR}}$  fields in the tree level mass eigenbasis  $\tilde{\chi}_i^-$ , and the on-shell renormalized fields  $\tilde{\chi}_i^{-P}$ ,

$$\begin{aligned} \psi_{iL}^- &= U_{ij}^\dagger \tilde{\chi}_{jL}^- = U_{ij}^\dagger (Z^L)_{jk}^{1/2} \tilde{\chi}_{kL}^{-P}, \\ \psi_{jR}^- &= V_{ij}^T \tilde{\chi}_{jR}^- = V_{ij}^T (Z^R)_{jk}^{1/2} \tilde{\chi}_{kR}^{-P}. \end{aligned} \quad (14)$$

We then introduce the effective mixing matrices of charginos, which are renormalization scale independent, and rewrite Eq. (13) by these matrices. We first define the effective mass matrix  $\overline{M}_C(p^2)$  in the  $\overline{\text{DR}}$  gauge basis as

$$\overline{M}_C(p^2) = M_C - \tilde{\Sigma}^D(p^2) - \frac{1}{2} M_C \tilde{\Sigma}^L(p^2) - \frac{1}{2} \tilde{\Sigma}^R(p^2) M_C. \quad (15)$$

$\tilde{\Sigma}_{ij}$  are chargino two-point functions  $\psi_i^+ \psi_j^-$  in the gauge basis. They are related to  $\Sigma$  in the  $\overline{\text{DR}}$  mass basis as

$$\begin{aligned} \Sigma^L &= U \tilde{\Sigma}^L U^\dagger, \\ \Sigma^R &= V^* \tilde{\Sigma}^R V^T, \\ \Sigma^D &= V^* \tilde{\Sigma}^D U^\dagger. \end{aligned} \quad (16)$$

$\overline{M}_C$  is diagonalized by two unitary matrices, the effective mixing matrices  $\overline{U}(p^2)$  and  $\overline{V}(p^2)$ , as

$$\overline{M}_D(p^2) = \overline{V}^*(p^2) \overline{M}_C(p^2) \overline{U}^\dagger(p^2), \quad (17)$$

where  $\overline{M}_D(p^2) = \text{diag}(\overline{m}_i(p^2))$  is a real diagonal matrix. Note that  $(\overline{M}_C, \overline{U}, \overline{V}, \overline{M}_D)$  are independent of the  $\overline{\text{DR}}$  renormalization scale  $Q$ .

We then give the forms of  $(\overline{U}, \overline{V})$  and  $\overline{M}_D$  in terms of two-point functions  $\Sigma(p)$  of charginos.  $(\overline{U}, \overline{V})$  are expanded as

$$\begin{aligned}\overline{U}(p^2) &= U + \delta U(p^2) = (1 + \delta u(p^2))U , \\ \overline{V}(p^2) &= V + \delta V(p^2) = (1 + \delta v(p^2))V .\end{aligned}\tag{18}$$

Here  $\delta u = \delta U \cdot U^\dagger$  and  $\delta v = \delta V \cdot V^\dagger$  must be anti-hermitian from the unitarity of  $(\overline{U}, \overline{V})$ . Their diagonal elements must be then pure imaginary.

The  $\mathcal{O}(\alpha)$  expansion of Eq. (17) gives

$$\begin{aligned}\overline{M}_D(p^2) &= (1 + \delta v^*(p^2))V^* \overline{M}_C(p^2)U^\dagger (1 + \delta u(p^2)) \\ &= M_D - \Sigma^D(p^2) - \frac{1}{2}M_D \Sigma^L(p^2) - \frac{1}{2}\Sigma^R(p^2)M_D \\ &\quad + \delta v^*(p^2)M_D + M_D \delta u(p^2) .\end{aligned}\tag{19}$$

The real parts of the diagonal elements of Eq. (19) give  $\overline{m}_i = m_i(\text{pole})$  at  $p^2 = m_i^2$ . The off-diagonal elements of Eq. (19) give the following relations

$$\begin{aligned}\delta u_{ij}(p^2) &= -\frac{1}{m_i^2 - m_j^2} \left( \frac{1}{2}(m_i^2 + m_j^2)\Sigma_{ij}^L + m_i m_j \Sigma_{ij}^R + m_i \Sigma_{ij}^D + m_j \Sigma_{ji}^{D*} \right) (p^2) , \\ \delta v_{ij}^*(p^2) &= -\frac{1}{m_i^2 - m_j^2} \left( \frac{1}{2}(m_i^2 + m_j^2)\Sigma_{ij}^R + m_i m_j \Sigma_{ij}^L + m_j \Sigma_{ij}^D + m_i \Sigma_{ji}^{D*} \right) (p^2) ,\end{aligned}\tag{20}$$

for  $i \neq j$ . Finally, the imaginary parts of diagonal elements give the relation

$$(-\delta u + \delta v^*)_{ii}(p^2) = \frac{1}{2m_i} [\Sigma^D - \Sigma^{D*}]_{ii}(p^2) .\tag{21}$$

By convention we set  $\delta v_{ii}(p^2) = 0$ . The relations Eq. (14) are then rewritten in terms of

$$U_{ij}^P \equiv \overline{U}_{ij}(m_i^2) , \quad V_{ij}^P \equiv \overline{V}_{ij}(m_i^2) ,\tag{22}$$

as

$$\begin{aligned}\psi_{iL}^- &= (U^P)_{ij}^\dagger (\delta_{jk} - \frac{1}{2}\Sigma_{jk}^L(m_k^2)) N_k^{1/2} \tilde{\chi}_{kL}^{-P} , \\ \psi_{iR}^- &= (V^P)_{ij}^T (\delta_{jk} - \frac{1}{2}\Sigma_{jk}^R(m_k^2)) N_k^{1/2} \tilde{\chi}_{kR}^{-P} , \\ N_k^{1/2} &= 1 - \frac{m_k^2}{2} [\Sigma_{kk}^{L'} + \Sigma_{kk}^{R'}] (m_k^2) - \frac{m_k}{2} [\Sigma_{kk}^{D'} + \Sigma_{kk}^{D'*}] (m_k^2) .\end{aligned}\tag{23}$$

$N_k^{1/2}$  is the real diagonal finite factor. The chargino wave function renormalization is then included by replacing  $U_{ik}^\dagger$  and  $V_{ik}^T$  in the couplings of the tree level amplitude by corresponding factors in Eq. (23), as

$$\begin{aligned}U_{ik}^\dagger &\rightarrow (U^P)_{ij}^\dagger (\delta_{jk} - \frac{1}{2}\Sigma_{jk}^L(m_k^2)) N_k^{1/2} , \\ V_{ik}^T &\rightarrow (V^P)_{ij}^T (\delta_{jk} - \frac{1}{2}\Sigma_{jk}^R(m_k^2)) N_k^{1/2} .\end{aligned}\tag{24}$$



The use of effective mixing matrices  $(U^P, V^P)$  has several nice features. First, the superficial singularity of  $\delta Z_{ij}$  for degenerate masses is completely absorbed into  $(U^P, V^P)$ . We can then see that the original singularity just reflects the arbitrariness in the diagonalization of a matrix with degenerate eigenvalues. The absence of this singularity is similar to the procedure proposed in Ref. [21]. Second, the renormalization scale dependence in Eq. (23) only appears in  $\Sigma^{L,R}$ . The  $Q$ -dependent parts of the first equation of Eq. (23) become, up to  $\mathcal{O}(\alpha)$ ,

$$\begin{aligned}\psi_{iL}^- &= (U^P)^\dagger_{ij} (\delta_{jk} - \frac{1}{2} \Sigma_{jk}^L |_{\text{div}}) \tilde{\chi}_{kL}^{-P} \\ &= (\delta_{ij} - \frac{1}{2} \tilde{\Sigma}_{ij}^L |_{\text{div}}) (U^P)^\dagger_{jk} \tilde{\chi}_{kL}^{-P} .\end{aligned}\quad (25)$$

Eq. (25) takes the same form as the  $SU(2) \times U(1)$  symmetric renormalization of  $\psi_i^-$ . This property is very convenient both in theoretical considerations of the renormalization and in numerical calculations. Note, however, that  $(U^P, V^P)$  are non-unitary at  $\mathcal{O}(\alpha)$ , unlike  $(U, V)$  and  $(\bar{U}, \bar{V})(p^2)^*$ .

The wave function corrections in our process are expressed as follows. By applying the rule in Eq. (24), the  $s$ -channel form factors  $i\Gamma_{ij}^{G\mu}$  in Eq. (6) are rewritten as

$$\begin{aligned}\Gamma_{ij}^{G\mu} &= -\gamma^\mu N_i^{1/2} N_j^{1/2} (\bar{v}_{Lij}^G P_L + \bar{v}_{Rij}^G P_R) \\ &\quad + \frac{1}{2} (\bar{v}_{Lij'}^G \Sigma_{j'j}^L(m_j^2) + \Sigma_{ii'}^{L\dagger}(m_i^2) \bar{v}_{Lij}^G) \gamma^\mu P_L + \frac{1}{2} (\bar{v}_{Rij'}^G \Sigma_{j'j}^R(m_j^2) + \Sigma_{ii'}^{R\dagger}(m_i^2) \bar{v}_{Rij}^G) \gamma^\mu P_R \\ &\quad + (\text{1PI vertex corrections}) ,\end{aligned}\quad (26)$$

where  $\bar{v}_{L(R)}^G$  are obtained from  $v_{L(R)}^G$  in Eq. (A.7) by replacing  $(U, V)$  by  $(U^P, V^P)$ . The  $Q$ -dependence of the second line of Eq. (26) exactly cancels that of the third line. The  $Q$ -independence of the rewritten form factor Eq. (26) is thus more transparent than the original form Eq. (6). Similarly, the last factor in the  $t$ -channel amplitude of Eq. (4) is rewritten as

$$\begin{aligned}V_{i1}^* V_{j1} + \frac{1}{2} (V_{i1}^{P*} V_{j'1} \delta Z_{j'j}^R + \delta Z_{ii'}^{R\dagger} V_{i'1}^* V_{j1}) \\ = V_{i1}^{P*} V_{j1}^P N_i^{1/2} N_j^{1/2} - \frac{1}{2} (V_{i1}^{P*} V_{j'1}^P \Sigma_{j'j}^R(m_j^2) + \Sigma_{ii'}^{R\dagger}(m_i^2) V_{i'1}^{P*} V_{j1}^P) .\end{aligned}\quad (27)$$

In leaving, we comment that the effective matrix method given here can be applied to any process involving on-shell charginos, since the corrections of Eq. (13) are universal. This method can also be extended to other particles with flavor mixing, such as the neutralinos.

### 2.3 Large $M_{\tilde{Q}}$ limit

We are interested in the limit where the squark mass  $M_{\tilde{Q}}$  is much larger than the masses of the charginos, the sneutrino, and the beam energy. Some corrections to the chargino production amplitude do not decouple in this limit but increase as  $\log M_{\tilde{Q}}$ . This reflects the supersymmetry breaking in the effective field theory below the squark mass scale [9].

---

\*The effective matrices are unitary up to corrections of  $\mathcal{O}((m_{\tilde{\chi}_2^{\pm}} - m_{\tilde{\chi}_1^{\pm}})/m_{\tilde{q}}^2)$ .

First, the effective chargino mass matrix  $\overline{M}_C(p^2)$  receives non-decoupling corrections. For  $M_{\tilde{Q}}^2 \gg p^2$  the effective mass matrix becomes independent of  $p^2$ . The asymptotic form is obtained by replacing the elements of the tree level mass matrix  $M_C$  of Eq. (A.2) by

$$M_2 \rightarrow M_2(Q) \left[ 1 + \frac{9g_2^2}{16\pi^2} \left( \ln \frac{M_{\tilde{Q}}}{Q} - \frac{1}{4} \right) \right] \equiv M_2^{\text{eff}}, \quad (28)$$

$$\mu \rightarrow \mu(Q) \left[ 1 + \frac{3(y_t^2 + y_b^2)}{16\pi^2} \left( \ln \frac{M_{\tilde{Q}}}{Q} - \frac{1}{4} \right) \right] \equiv \mu^{\text{eff}}, \quad (29)$$

$$\sqrt{2}M_W \cos \beta \rightarrow \sqrt{2}M_W \cos \beta(Q) \left[ 1 + \frac{\delta M_W}{M_W} + \frac{\delta \cos \beta}{\cos \beta} \right], \quad (30)$$

$$\sqrt{2}M_W \sin \beta \rightarrow \sqrt{2}M_W \sin \beta(Q) \left[ 1 + \frac{\delta M_W}{M_W} + \frac{\delta \sin \beta}{\sin \beta} \right], \quad (31)$$

where

$$16\pi^2 \frac{\delta \cos \beta}{\cos \beta} = \frac{3}{2} \sin^2 \beta \left( y_t^2 \ln \frac{M_W^2}{Q^2} - y_b^2 \ln \frac{M_{\tilde{Q}}^2}{Q^2} \right) - \frac{3}{2} y_b^2 \cos^2 \beta \ln \frac{M_{\tilde{Q}}^2}{M_W^2} + \frac{9}{4} y_b^2, \quad (32)$$

$$16\pi^2 \frac{\delta \sin \beta}{\sin \beta} = -\frac{3}{2} \cos^2 \beta \left( y_t^2 \ln \frac{M_{\tilde{Q}}^2}{Q^2} - y_b^2 \ln \frac{M_W^2}{Q^2} \right) - \frac{3}{2} y_t^2 \sin^2 \beta \ln \frac{M_{\tilde{Q}}^2}{M_W^2} + \frac{9}{4} y_t^2, \quad (33)$$

$$16\pi^2 \frac{\delta M_W}{M_W} = \frac{3}{2} g_2^2 \left( \ln \frac{M_{\tilde{Q}}^2}{M_W^2} + \frac{11}{12} \right) - \frac{1}{4} g_2^2 \left[ R(R+2) - (3R-2) \ln(R-1) + R^3 \ln \frac{R-1}{R} \right], \quad (34)$$

with  $R = m_t^2/M_W^2$ . The corrections to the diagonal elements can be absorbed into the effective mass parameters  $M_2^{\text{eff}}$  and  $\mu^{\text{eff}}$  and are not interesting within the context of the MSSM. By contrast, the corrections to the gaugino-Higgsino mixing masses cannot be absorbed into unknown parameters such as  $\tan \beta$ . The squark loop corrections to the effective mass matrix  $\overline{M}_C$ , and effective mixing matrices ( $U^P, V^P$ ), do not decouple in the large  $M_{\tilde{Q}}$  limit. This effect is very important if the gaugino-Higgsino mixing is not highly suppressed.

In the  $s$ -channel amplitude all other squark loop corrections decouple in this limit. The squark loop corrections from the gauge boson self energies  $\Pi^T$  decouple after the gauge couplings are renormalized. The factor  $N^{1/2}$  in Eq. (23) approaches to 1 in this limit. Finally, the non-decoupling terms in  $\Sigma^{L(R)}$  in Eq. (26) exactly cancel the  $F_{VL(R)}^G$  terms of the 1PI vertex corrections in Eq. (6). This result is consistent with the universality of gauge boson interactions.

By contrast, the  $\mathcal{O}(\log M_{\tilde{Q}})$  terms in  $\Sigma^{L(R)}$  remain in the  $t$ -channel amplitude and are very important. This is the origin of the ‘‘super-oblique corrections’’ discussed in Refs. [11, 12, 13]. We point out that the corrected  $t$ -channel amplitude takes a very simple form for sufficiently heavy squarks. In this case, the corrected amplitude is obtained from the tree level one by the replacement

$$\begin{aligned} g_2^2(Q) V_{i1}^* V_{j1} &\rightarrow g_2^2(Q) \left( 1 - \frac{1}{2} \tilde{\Sigma}_{11}^R(m_i^2) - \frac{1}{2} \tilde{\Sigma}_{11}^R(m_j^2) \right) V_{i1}^{P*} V_{j1}^P \\ &\equiv \bar{g}_{e\tilde{v}\tilde{W}}(m_i^2) \bar{g}_{e\tilde{v}\tilde{W}}(m_j^2) V_{i1}^{P*} V_{j1}^P. \end{aligned} \quad (35)$$

Here we used the fact that  $\tilde{\Sigma}_{1j'}^R(m_j^2)$  ( $j' \neq 1$ ) is insignificant for sufficiently heavy squarks. The parameter  $\bar{g}_{e\tilde{\nu}\tilde{W}}$ , which is renormalization scale independent, is interpreted as the effective  $e\tilde{\nu}\tilde{W}$  coupling.  $\bar{g}_{e\tilde{\nu}\tilde{W}}$  deviates from the corresponding gauge coupling,  $g_2^{\text{SM}}(Q)$ . Its asymptotic form is [11, 13],

$$\bar{g}_{e\tilde{\nu}\tilde{W}} = g_2^{\text{SM}}(Q) \left[ 1 + \frac{3g_2^2}{32\pi^2} \left( \ln \frac{M_{\tilde{Q}}^2}{Q^2} - \frac{3}{4} \right) \right]. \quad (36)$$

Here we note that the  $m_i^2$  dependence of  $\bar{g}_{e\tilde{\nu}\tilde{W}}(m_i^2)$  decouples in the large  $M_{\tilde{Q}}$  limit.

### 3 Numerical results

In this section we describe the dependence of the chargino production cross section  $\sigma(e^-e^+ \rightarrow \tilde{\chi}_1^- \tilde{\chi}_1^+)$  on various MSSM parameters. The production cross section is a function of the gauge couplings, the  $Z$ -boson and sneutrino masses, and the chargino masses and mixing matrices (parameterized by  $M_2$ ,  $\mu$ ,  $M_W$  and  $\tan\beta$ ). In the proposed colliders the electron beam can be highly polarized, therefore we often show the production cross section with a polarized electron beam. We denote the cross section as  $\sigma_{L(R)}$  when the initial state electron is left handed (right handed).

In the gaugino region ( $M_2 \ll |\mu|$ ),  $\tilde{\chi}_1^-$  is wino-like, and the amplitude receives both  $t$ -channel and  $s$ -channel contributions, unless the initial electron is right handed. If the electron is right handed, the  $t$ -channel amplitude vanishes because of the absence of a  $\tilde{W}e_R\tilde{\nu}$  coupling. In the opposite limit,  $|\mu| \ll M_2$ , the lightest chargino is Higgsino-like. Since the Higgsino couplings to the first and second generation (s)leptons are negligible, in the Higgsino limit only the  $s$ -channel amplitude contributes. Finally, when  $M_2 \sim |\mu|$ , both charginos have large gaugino and Higgsino components, and they are somewhat degenerate in mass. In this region of parameter space the chargino mixing matrices relevant in the production cross section are sensitive functions of  $\tan\beta$ , which enters in the off-diagonal elements of the chargino mass matrix.

Formulas for the one-loop corrected chargino production cross section are given in the previous section and the Appendix B, including quark and squark loop effects. The  $t$ -channel amplitude depends on the effective coupling  $\bar{g}_{e\tilde{\nu}\tilde{W}}$ , the effective chargino mixing matrices  $V^P$ , and decoupling corrections. The  $s$ -channel amplitude depends on the usual gauge couplings, the effective mixing matrices  $U^P, V^P$ , and decoupling corrections such as the 1PI gauge-chargino-chargino vertex correction.

Both amplitudes depend on squark masses  $m_{\tilde{q}_i}$ , squark mixing angles  $\theta_{\tilde{q}_i}$ , and quark-squark-gaugino(Higgsino) couplings. In this section, we present our results assuming a universal soft breaking squark mass  $M_{\tilde{Q}}$  and a universal trilinear coupling  $A$  at the weak scale. These parameters, along with  $\mu$  and  $\tan\beta$ , determine the squark masses and mixing angles. The third generation quark-squark-Higgsino couplings depend on the top and bottom Yukawa couplings  $y_t$  and  $y_b$ . As shown in Eqs. (30–34), the heavy top quark can give rise to a sizable correction proportional to  $y_t^2 \ln M_{\tilde{Q}}$ , which enters in the off-diagonal elements of the effective chargino mass matrix. The Yukawa couplings are also involved in the 1PI vertex corrections when the final state chargino is Higgsino-like. The top Yukawa coupling is very large when  $\tan\beta \rightarrow 1$  while  $y_b$  is substantial when  $\tan\beta \gtrsim 30$ .

In the following we will consider  $\tilde{\chi}_1^- \tilde{\chi}_1^+$  production in the three cases where the lightest chargino is predominantly gaugino, predominantly Higgsino, and in the mixed region. We will refer to the parameter sets listed in Table 1. We now discuss the three regions in turn.

name	description	$m_{\tilde{\chi}_1^-}$	$m_{\tilde{\chi}_2^-}$	$\tan \beta(M_Z)$	$m_{\tilde{\nu}}$	$A$	$\sqrt{s}$	$\text{sgn } \mu$
G1	gaugino region, $ \mu  > M_2$	200	800	2	100	0	500	-1
H1	Higgsino region, $ \mu  < M_2$	200	800	2	100	0	500	-1
G2	gaugino region, $ \mu  > M_2$	172	512	4	240	0	500	-1
H2	Higgsino region, $ \mu  < M_2$	172	512	4	400	0	500	-1
M	mixed region, $ \mu  < M_2$	172	255	4	240	0	500	-1

Table 1: Five parameter sets. All entries with mass units are in GeV.

### 3.1 Gaugino region

In Fig. 1(a) we plot the chargino production cross section  $\sigma(e^- e^+ \rightarrow \tilde{\chi}_1^- \tilde{\chi}_1^+)$  versus  $M_{\tilde{Q}}$  (solid line), for the G1 gaugino region parameter set of Table 1. In the gaugino (or Higgsino) region the diagonal elements of the effective chargino mass matrix  $\overline{M}_C$  are fixed by the input chargino masses, so they are independent of  $M_{\tilde{Q}}$ . Conversely, the  $\overline{\text{DR}}$  parameters  $M_2(M_2)$  and  $\mu(\mu)$  vary as  $M_{\tilde{Q}}$  increases. The effective mixing matrices  $U^P$ ,  $V^P$  contain non-decoupling  $\log(M_{\tilde{Q}}) + \text{constant}$  corrections. These corrections arise from corrections to the off-diagonal elements of the effective chargino mass matrix given in Eqs. (30–34). They contribute in both the  $s$ - and  $t$ -channel amplitudes. However, the dependence of the mixing matrices on the off-diagonal elements of the effective chargino mass matrix is suppressed for this set of parameters, so  $V_{11}^P$ ,  $U_{11}^P \simeq 1$  over the whole range of squark mass shown. The positive correction proportional to  $\log M_{\tilde{Q}}$  in Fig. 1(a) is therefore primarily due to the loop correction to the effective coupling  $\bar{g}_{e\nu\tilde{W}}$ .

The remaining corrections vanish in the large  $M_{\tilde{Q}}$  limit. These remaining corrections can be divided up into oblique and non-oblique parts, each of which satisfies decoupling. The non-oblique part consists of the 1PI vertex correction and the associated chargino wave function renormalization. In the following when we refer to the vertex correction we mean this combination. The vertex correction is somewhat complicated, so it is worthwhile checking whether this gauge and scale invariant correction can be neglected. The cross section calculated without including the vertex correction is shown by the dotted line in Fig. 1(a), and the ratio between the cross section without the vertex correction and the full one-loop cross section,  $\sigma_L^{\text{no-vtx}}/\sigma_L$ , is shown in Fig. 1(b). The maximum effect of the vertex correction is less than 0.5% of the total cross section for this choice of parameters. The vertex correction is negligible compared to the sensitivity to  $\sigma_L$  in future experiments.

As seen in Fig. 1(a), the left-handed cross section  $\sigma_L$  increases by about 14% as  $M_{\tilde{Q}}$  varies from 300 GeV to 3 TeV. The sensitivity to  $M_{\tilde{Q}}$  depends on  $m_{\tilde{\nu}}$  and  $\sqrt{s}$ , as discussed in Ref. [11].

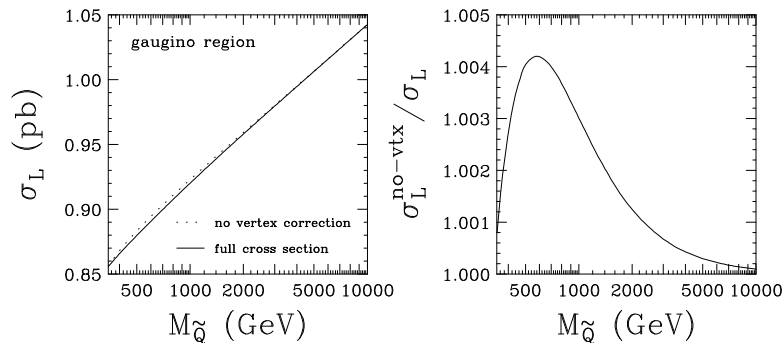


Figure 1: (a) The one-loop chargino production cross section  $\sigma_L$  as the function of the soft squark mass  $M_{\tilde{Q}}$  for the gaugino-like parameter set G1 of Table 1 (solid line). The positive correction proportional to  $\log M_{\tilde{Q}}$  is due to the loop correction to  $\bar{g}_{e\tilde{\nu}}\tilde{W}$ . The dotted line shows the cross section without the  $Z(\gamma)\tilde{\chi}^-\tilde{\chi}^+$  vertex corrections. (b) The ratio between the cross section without the gauge vertex corrections and the full one-loop cross section for the same set of parameters. The vertex correction is less than 0.5% of the total cross section.

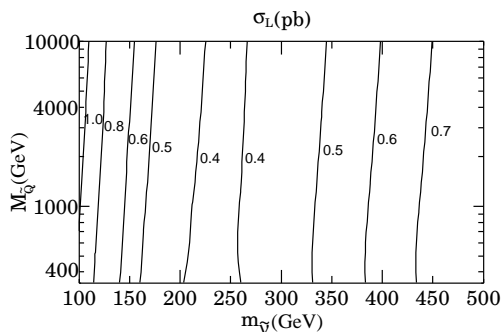


Figure 2: Contours of constant  $\sigma_L$  in the  $(M_{\tilde{Q}}, m_{\tilde{\nu}})$  plane for the parameter set G2 of Table 1.  $\sigma_L$  increases (decreases) with  $M_{\tilde{Q}}$  if  $m_{\tilde{\nu}} \lesssim 200$  GeV ( $\gtrsim 300$  GeV).

In Fig. 2 we show contours of constant  $\sigma_L$  in the  $(m_{\tilde{\nu}}, M_{\tilde{Q}})$  plane, for the G2 parameter set of Table 1. As  $M_{\tilde{Q}}$  increases,  $\sigma_L$  increases if  $m_{\tilde{\nu}}$  is less than 200 GeV, while it decreases if  $m_{\tilde{\nu}}$  is greater than 300 GeV. For  $m_{\tilde{\nu}} \sim 250$  GeV,  $\sigma_L$  becomes insensitive to  $M_{\tilde{Q}}$ . The dependence on  $M_{\tilde{Q}}$  from the  $t$ -channel amplitude is negligible in the limit  $m_{\tilde{\nu}} \gg \sqrt{s}$  since the  $t$ -channel amplitude scales as  $1/m_{\tilde{\nu}}^2$ .

### 3.2 Higgsino region

In Fig. 3 we show the  $M_{\tilde{Q}}$  dependence of  $\sigma_L$  when the chargino is Higgsino-like. We take parameter set H1 of Table 1. The diagonal elements of the effective chargino mass matrix  $\overline{M}_C$  are fixed by fixing the chargino masses. As in the gaugino region, the mixing is suppressed,  $|V_{12}|, |U_{12}| \simeq 1$ . The one-loop cross section including (not including) the vertex correction is shown by the solid (dotted) line. The cross section changes by less than 0.5% as  $M_{\tilde{Q}}$  varies from 300 GeV to 3 TeV. Such a weak  $M_{\tilde{Q}}$  dependence in Higgsino-like chargino production is expected from our observations in Sec. 2. Although the large top quark Yukawa coupling is involved, the vertex correction remains small, less than 1%.

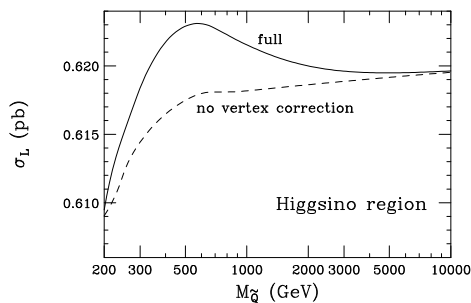


Figure 3: The cross section  $\sigma_L$  with/without the gauge vertex correction vs.  $M_{\tilde{Q}}$  for the parameter set H1 of Table 1 (solid/dotted). The lightest chargino is Higgsino-like. Both the dependence on  $M_{\tilde{Q}}$ , and the effect of the vertex correction is very weak.

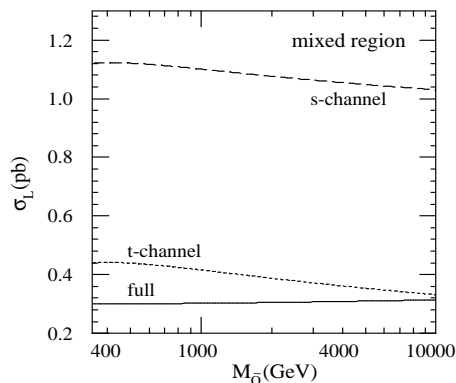


Figure 4:  $\sigma_L$  vs.  $M_{\tilde{Q}}$  for the mixed region parameter set M of Table 1 (solid). The  $s$ -channel and the  $t$ -channel cross sections are shown by the long dashed and short dashed lines. The cross section receives important corrections from the  $\log M_{\tilde{Q}}$  dependence of  $U^P$  and  $V^P$  (see text).

### 3.3 Mixed region

In the mixed region ( $M_2 \sim |\mu|$ ), the full one-loop cross section receives important corrections proportional to  $\log M_{\tilde{Q}}$  through the corrections to the effective mixing matrices  $U^P$ ,  $V^P$ , as well as  $\log M_{\tilde{Q}}$  corrections from the effective coupling  $\bar{g}_{e\tilde{\nu}\tilde{W}}$ . We illustrate this in Fig. 4, which shows the production cross section for parameter set M of Table 1. For this choice of parameters  $M_2$  and  $|\mu|$  are both near 200 GeV, so the chargino mass eigenstates are fully mixed ( $|V_{11}^P|^2 \simeq 0.6$ ). In the figure,  $\sigma_L$  increases by 4% as  $M_{\tilde{Q}}$  varies from 1 to 10 TeV (solid line). The destructive interference between the  $t$ -channel and  $s$ -channel amplitudes accounts for this insensitivity. The 22% reduction in the  $t$ -channel cross section (short-dashed line) is due to an 8% reduction of  $V_{11}^P$  and a 2% increase of  $\bar{g}_{e\tilde{\nu}\tilde{W}}$ . The  $s$ -channel cross section depends on both  $U^P$  and  $V^P$ , and decreases by 7% (long-dashed line).

### 3.4 Comparison of $M_{\tilde{Q}}$ and $\tan\beta$ dependencies

We now compare the  $M_{\tilde{Q}}$  and  $\tan\beta$  dependence of the chargino production cross section. In Figs. 5(a)–(e), we show contours of constant cross section in the  $(M_{\tilde{Q}}, \tan\beta)$  plane. In Fig. 5(a)

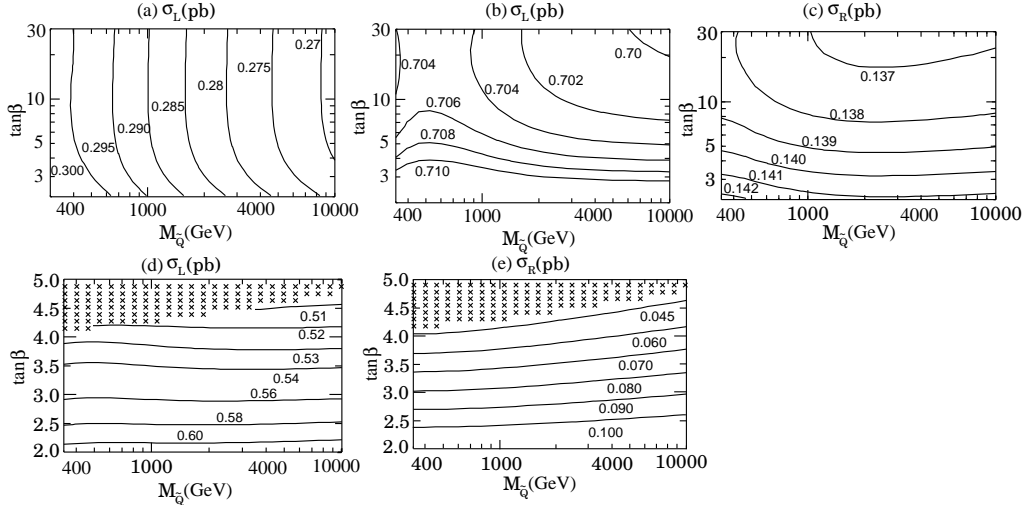


Figure 5: Contours of  $\sigma_L$  (Figs. (a), (b) and (d)) and  $\sigma_R$  (Figs. (c) and (e)) in the  $(M_{\tilde{Q}}, \tan\beta)$  plane. The parameter sets from Table 1 are (a) G2 (gaugino-like) with  $\sqrt{s} = 400$  GeV; (b) and (c) H2 (Higgsino-like); (d) and (e) M (mixed) with  $m_{\tilde{\nu}} = 400$  GeV. The  $M_{\tilde{Q}}$  dependence is strong in Fig. (e), though the  $\tan\beta$  dependence is more prominent. The cross hatched regions are excluded by the chargino mass constraints.

we use parameter set G2 of Table 1, with  $\sqrt{s} = 400$  GeV<sup>†</sup>. Since  $\tilde{\chi}_1^-$  is gaugino-like,  $\sigma_L$  depends on  $m_{\tilde{\nu}}$ . We see that  $\sigma_L$  is insensitive to  $\tan\beta$  in this case. It is almost constant in  $\tan\beta$  when  $\tan\beta > 5$ . On the other hand,  $\sigma_L$  decreases by 10% when  $M_{\tilde{Q}}$  changes from 300 GeV to 10 TeV due to the correction to  $\bar{g}_{e\tilde{\nu}\tilde{W}}$ .

In Figs. 5(b) and (c), we show the results for Higgsino-like  $\tilde{\chi}_1^-$ , using parameter set H2 of Table 1. Over the entire variation of  $\tan\beta$  and  $M_{\tilde{Q}}$  considered,  $\sigma_L$  varies by less than 1.5% (Fig. 5(b)). The cross section  $\sigma_R$  is relatively more sensitive to  $\tan\beta$  (Fig. 5(c)), but the absolute change in the cross section is smaller than in the  $\sigma_L$  plot. In both cases the  $M_{\tilde{Q}}$  dependence is very weak because of the very small mixing, and the absence of a  $t$ -channel coupling.

In the case of large gaugino-Higgsino mixing, the cross section is more sensitive to  $\tan\beta$  than to  $M_{\tilde{Q}}$ . In Figs. 5(d) and (e) we show the chargino production cross section in the mixed region, with parameter set M of Table 1, except  $m_{\tilde{\nu}} = 400$  GeV. The cross hatched region  $\tan\beta \gtrsim 4$  shown in these plots is excluded because it is not possible to obtain the specified chargino masses in this region. We find a strong dependence on  $\tan\beta$  for both  $\sigma_L$  (Fig. 5(d)) and  $\sigma_R$  (Fig. 5(e)). The  $M_{\tilde{Q}}$  dependence is very small in Fig. (d) due to the interference between the  $s$ - and  $t$ -channel amplitudes. In general it can be large. For example, in Fig. (e) at  $\tan\beta = 4$ ,  $\sigma_R$  changes from 45 fb to 62 fb as  $M_{\tilde{Q}}$  changes from 300 GeV to 10 TeV.

The large dependence of the one-loop cross section on  $M_{\tilde{Q}}$  in the mixed region is caused by the strong sensitivity of the cross section to the off-diagonal elements of the effective chargino mass matrix. In Ref. [7], it was claimed that a 4% measurement of  $\sigma_R$  results in the constraint  $3.9 < \tan\beta < 4.1$  (at  $\tan\beta = 4$ ). The tree level chargino masses were fixed in their determination. We see from Fig. 5(e) that for a given value of  $\sigma_R$  the central value of  $\tan\beta(M_Z)$  can shift by 0.5,

<sup>†</sup>The parameters are those used in Ref. [11]. We take  $\sqrt{s} = 400$  GeV for Fig. 5(a) because of the accidental insensitivity of  $\sigma_L$  to  $M_{\tilde{Q}}$  at  $\sqrt{s} = 500$  GeV.

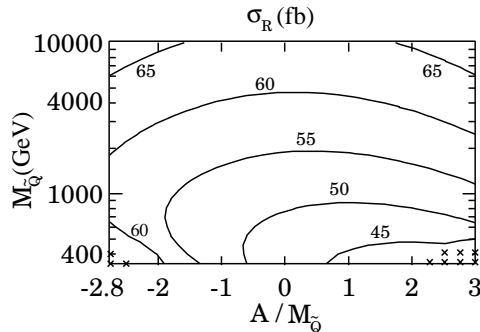


Figure 6: Contours of  $\sigma_R$  in the  $(A/M_{\tilde{Q}}, M_{\tilde{Q}})$  plane for the mixed region parameter set M of Table 1. The  $A/M_{\tilde{Q}}$  dependence is larger for smaller  $M_{\tilde{Q}}$ .

depending on  $M_{\tilde{Q}}$ .

We find that while the vertex correction is not substantial compared to the experimental sensitivity to the cross section, the corrections due to  $U^P$  and  $V^P$  can be. For example, the  $M_{\tilde{Q}}$  dependence in Fig. 5(e) is almost entirely due to  $U^P$  and  $V^P$ . At  $\tan\beta = 4$ ,  $\sigma_R$  changes by about 37% as  $M_{\tilde{Q}}$  varies from 300 GeV to 10 TeV. In contrast, the vertex correction is less than 1.4% over this range.

### 3.5 Squark mixing effects

Left-right squark mixing effects give rise to important corrections in the mixed region. The stop and sbottom mixing angles are controlled by  $A$ ,  $\mu$ , and  $\tan\beta$  as described in Appendix A. In Fig. 6 we show contours of constant  $\sigma_R$  in the  $(A/M_{\tilde{Q}}, M_{\tilde{Q}})$  plane for the chargino in the mixed region. We use parameter set M of Table 1. The cross hatched region of Fig. 6 is excluded either because of the chargino mass constraint or because  $m_{\tilde{t}}^2 < 0$ . The cross section shows strong dependence on  $A/M_{\tilde{Q}}$  when  $M_{\tilde{Q}}$  is small. For example, when  $A/M_{\tilde{Q}}$  varies from  $-2$  to  $+2$  with  $M_{\tilde{Q}} = 345$  GeV, the cross section changes from 61 fb to 39 fb. The stop mass eigenstates become fully mixed at large  $|A|/M_{\tilde{Q}}$ . The top squarks are well split when  $A/M_{\tilde{Q}} = -2$  ( $m_{\tilde{t}_1} = 128$  GeV,  $m_{\tilde{t}_2} = 528$  GeV), while at a point of small mixing,  $A/M_{\tilde{Q}} = 0.12$ , the top squarks are nearly degenerate ( $m_{\tilde{t}_1} = 383$  GeV,  $m_{\tilde{t}_2} = 386$  GeV). The  $A$  dependence of  $\sigma_R$  decouples at large  $M_{\tilde{Q}}$  as  $1/M_{\tilde{Q}}$  for fixed  $A/M_{\tilde{Q}}$ .

If only the two chargino masses and  $\sigma_R$  are measured it may not be possible to disentangle the dependence of the cross section on squark mixing from the dependence on  $\tan\beta$  and  $M_{\tilde{Q}}$ . For example, at  $M_{\tilde{Q}} = 345$  GeV in Fig. 6, we see the cross section is 61 fb at  $A/M_{\tilde{Q}} = -2$ . We can find the same cross section with the same chargino masses at  $A = 0$  by changing  $\tan\beta$  from 4 to 3.6. It may be necessary to measure  $A$  from other quantities. The stop masses and mixing angle can be constrained if  $m_{\tilde{t}_{1,2}}$  and  $\sigma(e^-e^+ \rightarrow \tilde{t}_1\tilde{t}_1^*)$  are measured [22]. Combining these measurements with measurements of  $\mu$  and  $\tan\beta$  from other processes,  $A_t$  can then be determined.

Because left-right squark mixing arises from  $SU(2) \times U(1)$  gauge symmetry breaking, it contributes to the violations of the relations between the tree level chargino and neutralino masses. We can utilize this dependence in efforts to constrain the values of  $A$  and  $\tan\beta$ . In Fig. 7 we show contours of  $A = 0$  varying  $\tan\beta$  and of  $\tan\beta = 4$  varying  $A$  in the  $(m_{\tilde{\chi}_3^0}, \sigma_R)$  plane (solid lines). We fix  $M_{\tilde{Q}} = 345$  GeV, and the other input parameters are fixed as in Fig. 6. The contours terminating at  $m_{\tilde{\chi}_3^0} = 201.4$  GeV have  $\tan\beta = 4$  while the contours terminating at  $m_{\tilde{\chi}_3^0} = 212.4$



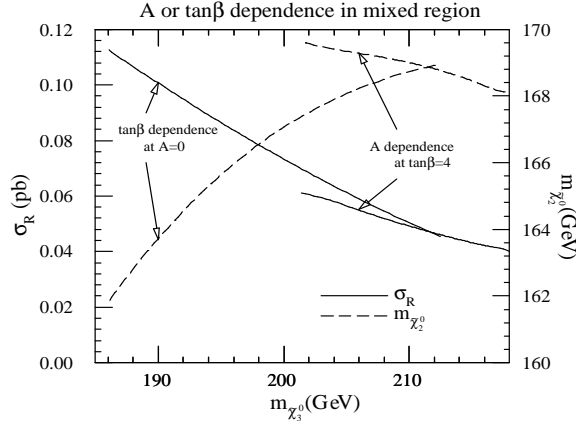


Figure 7: Contours of  $A = 0$  ( $\tan \beta = 4$ ) varying  $\tan \beta$  ( $A$ ) in the  $(m_{\tilde{\chi}_3^0}, \sigma_R)$  plane (solid lines), with  $M_{\tilde{Q}} = 345$  GeV. The variation of  $m_{\tilde{\chi}_2^0}$  with  $m_{\tilde{\chi}_3^0}$  for the same set of parameters is also shown (dashed lines).

GeV have  $A = 0$ . For values of  $\tan \beta$  slightly above 4, we cannot find solutions with the given chargino masses. For a given  $\sigma_R$ , we find  $m_{\tilde{\chi}_3^0}$  differs up to 3 GeV between two contours. We also show the variation of  $m_{\tilde{\chi}_2^0}$  with  $m_{\tilde{\chi}_3^0}$  when  $A$  or  $\tan \beta$  is varied (dashed lines). For fixed  $m_{\tilde{\chi}_3^0}$ ,  $m_{\tilde{\chi}_2^0}$  differs up to 2 GeV between the two curves. If we can measure the chargino and neutralino masses within 1 GeV or less, it could help to single out the effect of squark mixing <sup>‡</sup>.

Notice the squark mixing dependence of the radiative correction is mainly due to the correction to  $U^P$  and  $V^P$ , not the vertex correction. For example, at  $M_{\tilde{Q}} = 350$  GeV,  $\sigma_R$  changes from 47.3 fb to 41.0 fb as  $A/M_{\tilde{Q}}$  changes from 0 to 2, while the cross section without the vertex correction varies from 46.7 fb to 40.0 fb, a 1.4% to 2.4% effect. Although it is larger than the  $\lesssim 1\%$  effect found in the gaugino and Higgsino dominant regions, it is unimportant compared to the strong dependence of the cross section on  $A$ ,  $\tan \beta$ , and  $M_{\tilde{Q}}$ .

### 3.6 Comparison and approximations

We should briefly comment on the comparison of our results with those of Ref. [15]. The results in Ref. [15] are obtained by including top, stop, bottom and sbottom loops only. They underestimate the  $g_2^2 \log(M_{\tilde{Q}})$  corrections to  $\bar{g}_{e\nu\tilde{W}}/g_2$  and  $U^P$ ,  $V^P$ , which depend equally on the 1st and 2nd generation (s)quarks as the third generation. We have checked the  $t$ -channel exchange of the sneutrino has a substantial effect on the total cross section in some of their plots, and including the contributions of the first two generations significantly alters the results.

Our comparisons with their results show large numerical differences. For example, for the parameters corresponding to their Fig. 4 at  $\tan \beta = 0.5$ , we find the one-loop cross section *decreases* by 1.2% as  $M_{\tilde{Q}} = A^*$  varies from 200 to 1000 GeV. Their results show a 17% *increase* in the cross section. Notice they take the gaugino mass parameter  $M_2(M_Z)$  as input. Taking this unphysical

<sup>‡</sup>An excellent measurement of the chargino and neutralino masses may be achieved at proposed  $\mu^+\mu^-$  colliders. A recent study shows that it should be possible to measure the lighter chargino mass with an accuracy of 30 to 300 MeV by measuring the cross section in the threshold region [23].

\*We refer to their  $A$ . We use the opposite sign convention for  $A$ .

mass parameter as input generally leads to larger  $M_{\tilde{Q}}$  dependence. In the example just mentioned, taking  $m_{\tilde{\chi}_2^-}$  as input reduces the  $M_{\tilde{Q}}$  dependence from 1.2% to 0.4%.

We also find smaller differences between the tree level and one-loop cross sections. However, this is not surprising, since the definition of the tree level cross section is somewhat arbitrary. Our tree level cross section is determined by the two chargino masses,  $M_W$ ,  $M_Z$ ,  $m_{\tilde{\nu}}$ ,  $\tan\beta$ , and the effective theory (i.e. standard model)  $\overline{\text{MS}}$  gauge couplings. The tree level cross section depends on the choice of the scale of the effective theory gauge couplings. An appropriate scale is found by considering the Higgsino production cross section in the limit  $M_Z \ll \sqrt{s} \ll M_{\tilde{Q}}$ . In this limit the squarks are completely decoupled. Because of the constant correction in the quark loop oblique correction, the cross section in the effective theory is equal to the cross section in the full theory if the effective theory gauge couplings are evaluated at the renormalization scale  $Q = \exp(-5/6)\sqrt{s} \simeq \sqrt{s}/2$ . Hence, our tree level cross section is evaluated with effective theory gauge couplings evaluated at the scale  $\sqrt{s}/2$ . With this choice, the tree level and full one-loop cross sections are nearly equal when the squark corrections decouple.

We have already discussed that, for practical purposes, it is safe to neglect the vertex correction. We will now consider two approximations to the remaining corrections. In the first, the effective theory approximation (ETA), we use the effective coupling  $\bar{g}_{e\tilde{\nu}\tilde{W}}$  and the effective mixing matrices,  $U^P$ ,  $V^P$ . In this approximation some  $1/M_{\tilde{Q}}^2$  corrections are included. In the second approximation, the “log + constant” approximation (LCA), we strictly keep only the non-decoupling squark corrections, i.e. we include only the corrections of the form  $\log(M_{\tilde{Q}}) + \text{constant}$ . The effective coupling in the log + constant approximation,  $\bar{g}_{\text{LCA}}$ , is given in Eq. (36). The effective mixing matrices in the LCA are found as follows. The off-diagonal elements of the effective chargino mass matrix in the LCA are given in Eqs. (30–34). The effective mixing matrices in the log + constant approximation,  $U_{\text{LCA}}^P$ ,  $V_{\text{LCA}}^P$ , are then determined from the two chargino masses and these off-diagonal elements. Notice that  $\bar{g}_{\text{LCA}}$ ,  $U_{\text{LCA}}^P$ ,  $V_{\text{LCA}}^P$ , and the effective theory couplings, are renormalization scale independent.

In Fig. 8 we show the ratio of the various approximations to the full cross section, versus  $M_{\tilde{Q}}$ . We plot the ratio of unpolarized cross sections in the gaugino, Higgsino, and mixed regions in Figs. 8(a), (b), and (c), with parameter sets G1, H1 and M of Table 1, respectively. The cross section without the vertex correction is shown by the dotted line. The ETA result is shown with the dot-dashed line, and the LCA result is indicated by the dashed line.

There are two factors which contribute to the deviations from unity in the large  $M_{\tilde{Q}}$  region in the ETA and LCA results. For one, these approximations are calculated with effective theory couplings, while the full calculation is calculated with full theory couplings. This mismatch causes discrepancies of order  $(\alpha \log M_{\tilde{Q}})^2$ . These discrepancies give some indication of the expected magnitude of two-loop corrections. Another reason why the approximations can disagree in the large  $M_{\tilde{Q}}$  limit is that the scale used to evaluate the  $s$ -channel tree level gauge couplings is  $\sqrt{s}/2$ . The scale which should be used to get exact agreement in the decoupled regime is somewhat different, depending on  $M_Z$ ,  $m_t$ , and  $\sqrt{s}$ .

In all three figures the vertex correction is less than 1%, so the “no vertex” approximation is a good one, even for very small squark masses. The ETA also works well, better than 1% except at  $M_{\tilde{Q}} \lesssim \sqrt{s}/2$  in Fig. (b). The LCA works as well as the ETA, except in the gaugino region with

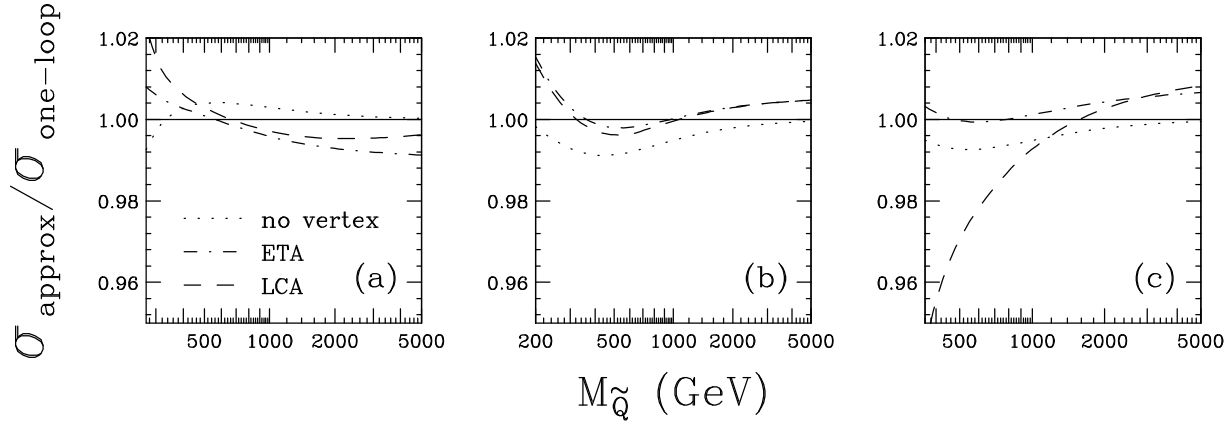


Figure 8: Various approximations to the cross section divided by the full one-loop cross section. The results for the “no vertex” approximation, effective theory approximation (ETA), and “log + constant” approximation (LCA) are shown. Figures (a), (b) and (c) show results in the gaugino, Higgsino, and mixed regions of parameter space, respectively. (Parameter sets G1, H1, and M of Table 1 are used.)

$M_{\tilde{Q}} \lesssim \sqrt{s}$  and in the mixed region with  $M_{\tilde{Q}} \lesssim 1.5\sqrt{s}$ . By comparing the ETA and LCA results we see that the  $1/M_{\tilde{Q}}^2$  corrections included in  $\bar{g}_{e\tilde{\nu}\tilde{W}}$ ,  $U^P$  and  $V^P$  can be essential in obtaining a good approximation, even for squark masses as large as  $1.5\sqrt{s}$ .

## 4 Uncertainty in the chargino production cross section measurement

### 4.1 Previous analyses

In this section we revisit previous studies of chargino production and decay [7, 11]. Chargino production can be studied in  $e^+e^-$  collider experiments by observing their decay into  $\nu\ell\tilde{\chi}_1^0$  or  $q\bar{q}'\tilde{\chi}_1^0$ , with signals  $\ell 2j$  + missing momentum or  $4j$  + missing momentum.

In Refs. [7, 11] the probe of the supersymmetric relation of  $SU(2)$  gauge/gaungino couplings  $g_2^{\text{SM}} = \bar{g}_{e\tilde{\nu}\tilde{W}}$  was considered based on the MC study of the  $\ell 2j$  mode at the point in parameter space  $(\mu, M_2, \tan\beta, M_1/M_2, m_{\tilde{\nu}}) = (-500 \text{ GeV}, 170 \text{ GeV}, 4, 0.5, 400 \text{ GeV})$ , where  $m_{\tilde{\chi}_1^+} = 172 \text{ GeV}$  and  $m_{\tilde{\chi}_1^0} = 86 \text{ GeV}$ . The analysis of Ref. [7] assumes  $\sqrt{s} = 500 \text{ GeV}$  and that no direct production of  $\tilde{\nu}$  is available. This results in a poor constraint on  $\bar{g}_{e\tilde{\nu}\tilde{W}}$ . In Ref. [11] the authors consider the same point in parameter space, except they assume  $m_{\tilde{\nu}}$  is measured directly, and  $\sqrt{s}$  can be tuned. Further, they assume that the uncertainty of the theoretical input parameters in the chargino and neutralino sector, the acceptance of  $\ell 2j$  events, and the dependence of the acceptance on the theoretical input parameters are independent of  $m_{\tilde{\nu}}$  and  $\sqrt{s}$ . Under these assumptions, they find  $\delta\bar{g}_{e\tilde{\nu}\tilde{W}}/g_2^{\text{SM}} = 2\%$  with  $m_{\tilde{\nu}} = 240 \text{ GeV}$  and  $\sqrt{s} = 400 \text{ GeV}$ . This result is considerably poorer than the result  $\delta\bar{g}_{e\tilde{\nu}\tilde{W}}/g_2^{\text{SM}} < 0.6\%$ , estimated in the sneutrino production study of Ref. [13].

The purpose of this section is to provide a critical discussion of the analysis of Refs. [7, 11]. We point out that the poor constraint found in Ref. [11] results from the low acceptance of the  $\ell 2j$  mode (found in Ref. [7]), and the low acceptance is further traced back to the (special) choice of parameters. We also point out that the signal acceptance and dependence of the acceptance on the theoretical input parameters can be strongly dependent on  $\sqrt{s}$ . Therefore the estimate given

in Ref. [11] cannot be trusted at other values of  $\sqrt{s}$  unless a dedicated MC simulation is provided for both the signal and background. The bottom line is that the constraint on  $\bar{g}_{e\tilde{\nu}}\tilde{W}$  can be greatly improved for more generic parameters, and by optimizing the beam energy and cuts.

Before going into the details of their simulation, we shall discuss the background to the  $\ell 2j$  signal for the case where  $\tilde{\chi}_1^\pm$  decays exclusively into  $\tilde{\chi}_1^0 W$  as follows

$$\begin{aligned} e^+e^- &\rightarrow \tilde{\chi}_1^+\tilde{\chi}_1^- \\ &\rightarrow W^+W^-\tilde{\chi}_1^0\tilde{\chi}_1^0 \\ &\rightarrow l\nu q\bar{q}' + \cancel{p}_T . \end{aligned}$$

We assume  $\tilde{\chi}_1^0$  is the stable LSP, so it escapes detection and (along with the neutrino) gives rise to missing momentum in these events.

This process suffers from  $W$ -boson pair production background. In the background events the total momentum of the  $W$ -boson pair is balanced in the transverse direction, but the observed transverse momentum is not balanced, due to the escaping neutrino. Hence, the discrimination between the signal and background is difficult.

In the MC study of Ref. [7], the following cuts are made to reduce the background from  $W$ -boson pair production in the  $\ell 2j$  mode:

- a) existence of an isolated hard lepton;  $E_\ell > 5$  GeV,  $\theta_{q\ell} > 60^\circ$
- b)  $\cancel{p}_T > 35$  GeV
- c)  $\theta_{\text{acop}} > 30^\circ$
- d)  $m_{\ell\nu\text{ISR}} > 120$  GeV
- e)  $-Q_\ell \cos\theta_{\text{had}}, Q_\ell \cos\theta_\ell < 0.707$

Cuts b), c) and d) are set to reduce the  $W$ -pair events produced nearly back to back in the transverse direction, while keeping the supersymmetric signal. The cut e) is designed to remove the large forward peak of the  $WW$  events.

Although these cuts are standard ones to improve the signal to noise ratio, the acceptance of the signal turns out to be small,

$$\eta = \frac{N_{\text{obs}}}{\sigma_L B_l B_h \mathcal{L}} = 11.9\% , \quad (37)$$

resulting in  $S/N = 1$  at the previously mentioned point in parameter space.

Our knowledge of the acceptance is limited by the errors of the underlying parameters ( $\mu$ ,  $M_1$ ,  $M_2$ ,  $\tan\beta$ ,  $m_{\tilde{\nu}}$ ). The systematic errors on  $\eta$  are estimated as  $\Delta\eta_{\text{sys}} = 0.55\%$  by allowing the underlying parameters to vary so that  $m_{\tilde{\chi}_1^+}$ ,  $m_{\tilde{\chi}_2^+}$ , and  $m_{\tilde{\chi}_1^0}$  vary within 2 GeV of their input values.

While  $\Delta\eta_{\text{sys}}$  itself is small, the error in the cross section due to the acceptance uncertainty turns out to be large, i.e.  $\Delta\eta/\eta = 5\%$ . This is comparable to the change in the cross section when  $m_{\tilde{q}}$  changes from 1 TeV to 4.5 TeV with  $m_{\tilde{\nu}} = 240$  GeV and  $\sqrt{s} = 400$  GeV.

No question was raised concerning the small acceptance of the  $\ell 2j$  mode in Refs. [7, 11], but the value should be contrasted with other MC studies, which generally claim acceptances of 30 to 50% for SUSY signals [4, 6, 24]. The low acceptance in Eq. (37) is a consequence of the special choice of parameters. At the point in question,  $m_{\tilde{\chi}_1^+} = 172$  GeV, and  $m_{\tilde{\chi}_1^0} = 86$  GeV, so the mass difference between the parent and the daughter particles  $\Delta m = m_{\tilde{\chi}_1^+} - m_{\tilde{\chi}_1^0} - m_W$  is only 6 GeV. In the rest frame of  $\tilde{\chi}_1^+$ , both the  $W$ -boson and  $\tilde{\chi}_1^0$  are nonrelativistic. When the parent  $\tilde{\chi}_1^+$  is boosted, the angle between the  $\tilde{\chi}_1^+$  momentum and the  $W$ -boson, and also the momentum spread of the  $W$ , can be very small. When the charginos are produced at  $\sqrt{s} = 500$  GeV,  $\theta_{\tilde{\chi}_1^+ W} < 15^\circ$ , and the  $W$ -boson pair momenta and  $\tilde{\chi}_1^0$  momenta are roughly balanced.

Notice in the cuts listed above we are relying on large  $\theta_{\tilde{\chi}_1^+ W}$  and large missing transverse momentum to separate the signal from the  $WW$  background, but neither of these attributes are characteristic of the signal events. The small acceptance merely results from the fact that the  $W$  pair from the signal and the background have very similar kinematics at this particular point in parameter space.

The small acceptance has a direct effect on the acceptance uncertainty. The signal event distribution in the  $(\cancel{p}_T, \theta_{\text{acop}}, m_{\ell\nu})$  space sits near the background distribution and therefore near the cut region. When the input parameters are changed slightly within their error, the signal region also changes in the  $(\cancel{p}_T, \theta_{\text{acop}}, m_{\ell\nu})$  space. Because the accepted number of events for the input parameters is so small compared to the total number of reconstructed  $W$ -pair events, a small change in the signal region easily changes the acceptance by several percent. Relatedly,  $\theta_{\tilde{\chi}_1^+ W}$  is a rather sensitive function of  $\Delta m$  when  $\Delta m$  is small. Note that the systematic error of the acceptance is estimated by changing  $\Delta m$  from 2 to 10 GeV in Ref. [7].

To illustrate the kinematics, we show the acoplanarity angle distribution of  $W$  pairs reconstructed from  $e^+e^- \rightarrow \tilde{\chi}_1^+ \tilde{\chi}_1^- \rightarrow WW \tilde{\chi}_1^0 \tilde{\chi}_1^0 \rightarrow 4j + \cancel{p}_T$  events in Fig. 9. The  $4j$  mode also suffers from the  $WW$  background, however the cuts to remove the SM background are far simpler than those of the  $\ell 2j$  mode<sup>†</sup>.

Fig. 9 shows the acoplanarity angle distribution after applying the cuts to reject background  $W$ -pairs given in Ref. [6], except for the acoplanarity angle cut  $\theta_{\text{acop}} > 30^\circ$ . To generate MC events, we modified the event generator of Ref. [6], and we used the JLC detector simulator [6]. The effect of initial state radiation is included. The distribution shown by points with error bars corresponds to our standard input parameters  $(\mu, M_1, M_2, \tan\beta, m_{\tilde{\nu}}) = (-500 \text{ GeV}, 84.6 \text{ GeV}, 170 \text{ GeV}, 2, 400 \text{ GeV})$ , resulting in  $m_{\tilde{\chi}_1^+} = 176.6$  GeV and  $m_{\tilde{\chi}_1^0} = 86.9$  GeV. The parameters are chosen so that  $\Delta m = 9.4$  GeV, larger than that in Ref. [7]. The size of the error bars and the central values are determined from 10000 generated events, corresponding to  $\int \mathcal{L} dt = 16 \text{ fb}^{-1}$ . On this same plot we also show two distributions corresponding to  $M_1 = 90.6$  GeV (short-dashed) and  $M_1 = 78.6$  GeV (long-dashed). These distributions correspond to  $m_{\tilde{\chi}_1^0} = 92.2$  GeV and  $m_{\tilde{\chi}_1^0} = 80.3$  GeV, respectively. The difference in  $\Delta m$  for these two curves is 12 GeV, large enough to create a statistically significant difference in the event distribution, given the somewhat small integrated luminosity we are considering. These curves are normalized to have equal numbers of events<sup>‡</sup>.

<sup>†</sup>The  $4j$  mode suffers from the SUSY background due to  $e^+e^- \rightarrow \tilde{\chi}_2^0 \tilde{\chi}_2^0 \rightarrow 4j \tilde{\chi}_1^0 \tilde{\chi}_1^0$ , which may be hard to distinguish from the chargino signal. We discuss the  $4j$  mode here for more or less illustrative purposes, although it is possible to extract more physics information by including this mode in a combined fit.

<sup>‡</sup>The total number of reconstructed  $WW$  events depends on the chargino/neutralino mass differences. For

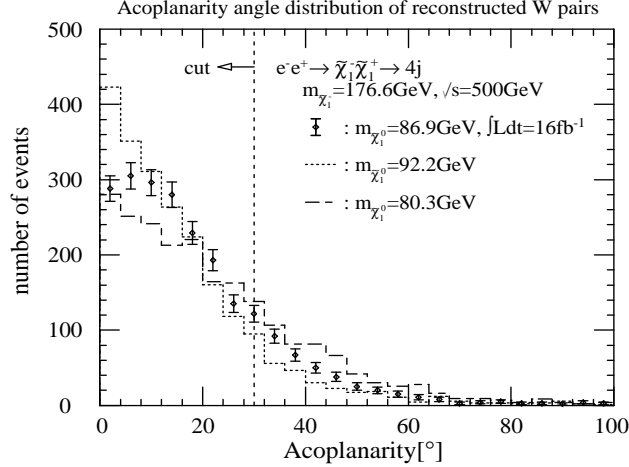


Figure 9: The number of accepted chargino production events vs. the acoplanarity angle, with  $\sqrt{s} = 500$  GeV and  $\int \mathcal{L} dt = 16 \text{ fb}^{-1}$ . The points with error bars are for  $M_1 = 84.6$  GeV, and the long-dashed (short-dashed) line corresponds to  $M_1 = 78.6$  (90.6) GeV. See text for other parameters.

The acceptance changes drastically for the different cases. Implementing  $\theta_{\text{acop}} > 30^\circ$ , we find the acceptance varies by a factor of two. The acceptance is correlated with  $\Delta m$ , which determines the maximal  $\tilde{\chi}^+ W$  angle. Below we list  $\Delta m$ , the maximal angle  $\theta_{\tilde{\chi}^+ W}^{\text{max}}$ , and the acceptance for the three cases.

$m_{\tilde{\chi}_1^0}$	$\Delta m$	$\theta_{\tilde{\chi}^+ W}^{\text{max}}$	$\eta$
92.2 GeV	4.1 GeV	$13.7^\circ$	14.1 %
86.9 GeV	9.4 GeV	$20.7^\circ$	19.3 %
80.3 GeV	16.0 GeV	$27.2^\circ$	27.3 %

Varying  $m_{\tilde{\chi}_1^0}$  by 2%, we expect about a 2% change in the acceptance. This corresponds to  $\Delta\eta/\eta$  of about 10%.

Notice we require  $\theta_{\text{acop}} > 30^\circ$  to reduce the SM background, while the maximal  $\theta_{\text{acop}}$  is  $2\theta_{\tilde{\chi}^+ W}^{\text{max}}$  if the reconstructed jet momenta are identified with the quark momenta. For the sample with  $\Delta m = 4.1$  GeV, the events are accepted by virtue of the finite resolution of the jet axis. As  $\theta_{\tilde{\chi}^+ W}$  increases above half of the acoplanarity angle cut, the accepted number of events increases linearly with  $\theta_{\tilde{\chi}^+ W}$ . On the other hand, if  $\Delta m$  is so large that  $\theta_{\tilde{\chi}^+ W}^{\text{max}} \gg \theta_{\text{acop}}$ , then most of the events pass the cut by a wide margin. In particular, most events are accepted regardless of several percent variations in the input parameters. Therefore, the acceptance error is much smaller in a generic region of parameter space. We expect the acceptance uncertainty to scale roughly inversely with the acceptance, for sufficiently large  $\Delta m$ . We will examine this conjecture later by an explicit example. The uncertainty itself depends on the mode under consideration and the cuts applied, as we discuss in the next subsection.

For the  $\ell 2j$  mode the situation is less clear. Each of the three cuts, the  $\cancel{p}_T$  cut, the acoplanarity angle cut, and the  $m_{\ell\nu}$  cut, causes roughly the same reduction in the number of signal events.

example, rejection of the forward going jets ( $W$ 's) gives such dependences. However, as discussed below, this mass sensitivity is small compared to the uncertainty in the acceptance due to the acoplanarity angle cut.

Because of the missing momentum from the escaping neutrino, each cut yields smaller reductions compared to the  $4j$  mode. However, each acceptance dominantly depends on the parameter  $\Delta m$ . In particular, the acceptance is larger for larger  $\Delta m$  for all of these cuts. When  $\Delta m$  is small the signal region significantly overlaps the background region. In that case, as with the  $4j$  mode, the variation of  $\Delta m$  within the error is largely responsible for causing events to move into and out of the accepted region.

## 4.2 Improving the measurement

We found in the previous subsection that the point in parameter space considered in Refs. [7, 11] must be regarded as a pessimistic case. At other points the acceptance will generically increase, leading to a decrease in the acceptance uncertainty. However, nature may equally well choose any point, so let us reconsider this point for a moment, and seek a procedure to reduce the acceptance uncertainty.

One possibility is to reduce the chargino and neutralino mass errors, especially the error on their mass difference. When there is no correlation between  $\delta m_{\tilde{\chi}_1^+}$  and  $\delta m_{\tilde{\chi}_1^0}$ , the largest (smallest) acceptance comes from the point where  $m_{\tilde{\chi}_1^+} - m_{\tilde{\chi}_1^0}$  becomes maximum (minimum) within the mass errors. For example, in the  $4j$  mode, when we change  $M_1$  and  $M_2$  so that  $(\Delta m_{\tilde{\chi}_1^+}, \Delta m_{\tilde{\chi}_1^0}) = (+2 \text{ GeV}, -2 \text{ GeV})$ , we find the acceptance increases by 6%. With  $(\Delta m_{\tilde{\chi}_1^+}, \Delta m_{\tilde{\chi}_1^0}) = (+2 \text{ GeV}, +2 \text{ GeV})$  we find the acceptance increases by 1.7%<sup>§</sup>. Hence, the acceptance is over three times more sensitive to absolute changes in the mass difference than the mass sum.

In the standard technique to determine a particle's mass from the energy distribution of one of the daughter particles in two body decay, the mass difference between the parent and the daughter particle is measured better than the individual masses, especially when the parent particle is significantly boosted. (See examples in Refs. [6, 24].) So, at generic points the uncertainty in the acceptance is much smaller than one would expect from uncorrelated mass errors. However, in this particular example, the acceptance is smaller near the endpoints of the energy distribution. This is because the daughter particle has a maximal energy when it goes in the same direction as the parent particle. In such a case, the acoplanarity of the event comes only from the other chargino, leading to small statistics near the endpoints. Therefore, we expect that the energy distribution is less sensitive to the chargino/neutralino mass difference for the case given in Ref. [7].

The uncertainty of the acceptance may be reduced by increasing the acceptance itself. One can increase the acceptance easily in the  $4j$  mode by reducing  $\sqrt{s}$ . In Fig. 10 we see the acoplanarity angle distribution of  $W$ -pairs is much flatter for  $\sqrt{s} = 400 \text{ GeV}$ . The angle  $\theta_{\tilde{\chi}_1^+ W}^{\max} = 41.3^\circ$ , so a large number of events pass the cut  $\theta_{\text{acop}} > 30^\circ$ . We find the acceptance increases to 54.8% from 19.3% at our standard point (where  $m_{\tilde{\chi}_1^+} = 176.6 \text{ GeV}$  and  $m_{\tilde{\chi}_1^0} = 86.9 \text{ GeV}$ ). The acceptance increases by 2.4% with  $m_{\tilde{\chi}_1^+} = 176.6 + 2 \text{ GeV}$  and  $m_{\tilde{\chi}_1^0} = 86.9 - 2 \text{ GeV}$ . The uncertainty in the acceptance from the chargino/neutralino mass errors is therefore reduced by factor of 7 relative to the  $\sqrt{s} = 500 \text{ GeV}$  case<sup>¶</sup>.

---

<sup>§</sup>At  $(+6 \text{ GeV}, +6 \text{ GeV})$  we find the acceptance is 24.3%. We then assume a linear dependence on the  $\Delta m_{\tilde{\chi}}$  to obtain the estimate for  $(+2 \text{ GeV}, +2 \text{ GeV})$ .

<sup>¶</sup>However, we find the acceptance error including the  $WW$  reconstruction efficiency is only reduced by a factor of 2.6. The dependence of the  $W$ -pair reconstruction efficiency on the chargino/neutralino masses comes in through

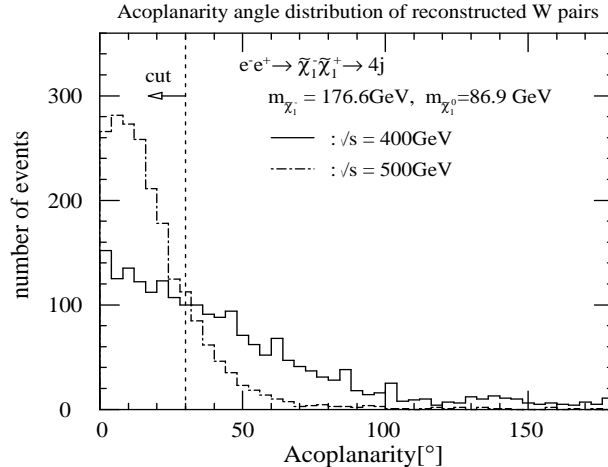


Figure 10: The acoplanarity angle distribution of  $W$ -pair events from chargino production, at  $\sqrt{s} = 400$  GeV. See the text for other parameters and cuts.

For the  $\ell 2j$  mode, reducing  $\sqrt{s}$  may not result in a larger acceptance. For this mode, many cuts are needed to reduce backgrounds and the relevant distributions have different  $\sqrt{s}$  dependencies. For example, the  $\cancel{p}_T > 35$  GeV cut rejects more events at smaller  $\sqrt{s}$ , because the narrower allowed range of  $\tilde{\chi}_1^0$  momentum leads to observed events which are more balanced in transverse momentum. Since the  $WW$  background also has a softer  $\cancel{p}_T$  at smaller  $\sqrt{s}$ , it may be beneficial to reduce the  $\cancel{p}_T$  cut. To determine to what extent the acceptance can be improved, both the signal and background must be studied carefully, because the signal to noise ratio is near unity in this mode. Such a study is beyond the scope of this paper.

We summarize this section as follows.

- The previously claimed cross section error due to the uncertainty in the acceptance should not be taken as a generic statement. The point studied in Ref. [7] has special kinematic properties making it a very pessimistic case.
- Because the error in the acceptance scales inversely with the acceptance, the acceptance uncertainty may be minimized by changing the beam energy and the cuts so as to maximize the acceptance. One should always try to find the best possible way to increase the acceptance, not in order to increase the statistics, but rather to reduce the systematic error.
- If it is clear that specific distributions and/or cuts are the dominant source of the uncertainty, one might benefit from fitting the distribution. Fig. 9 illustrates an example where the shape of the acoplanarity angle distribution (not its overall normalization) changes substantially with  $\Delta m$ .

---

the dependence on the  $W$ -boson velocity. The daughter  $W$ -boson in the center of mass frame is substantially nonrelativistic at  $\sqrt{s} = 400$  GeV, so the  $W$ -boson velocity is sensitive to the chargino/neutralino mass difference. This dependence may be ascertained on an event by event basis.



## 5 Discussion and conclusions

In this paper we calculated the chargino production cross section including full one-loop quark and squark loop corrections. Quark and squark loop corrections are known to induce corrections proportional to  $\log m_{\tilde{q}}$ . This logarithmic correction is seen as a reflection of broken supersymmetry in the effective theory below the squark mass scale. The correction may be observable in chargino, neutralino, and slepton production and decay processes as discussed in Refs. [11, 13]. In this paper, the important corrections in the large  $m_{\tilde{q}}$  limit were extracted from the full one-loop calculation, and they were compared with the decoupling corrections. We also revisited previous MC studies of the measurement of the correction to the fermion-sfermion-chargino coupling  $\delta g = \bar{g}_{e\nu\tilde{W}} - g_2^{\text{SM}}$ . In Ref. [11] it was stated that a precise determination of the chargino production cross section is important, but the uncertainty in the theoretical underlying parameters would be the limiting factor in the measurement. In this paper we pointed out the systematic error will not be a problem at generic points in MSSM parameter space. This is contrary to their remarks which were based on a MC study at a point in parameter space with special kinematic properties. Our study shows that experiments at future  $e^+e^-$  colliders should be sensitive to the squark mass scale if the chargino is produced with a large cross section.

We presented our one-loop calculation in terms of the renormalization scale independent effective chargino mixing matrices,  $U^P$  and  $V^P$ . They are the matrices which diagonalize the effective mass matrix  $\overline{M}_C(p^2)$  at momentum  $p^2 = m_{\tilde{\chi}^-}^2$ . When the one-loop amplitude is written in terms of  $U^P$  and  $V^P$ , a complicated part of the wave function renormalization is absorbed, and the remaining part is a simple expression. The sum of the 1PI gauge- $\tilde{\chi}^- \tilde{\chi}^+$  vertex correction and the remaining simplified wave function renormalization is scale independent, and decouples in the large  $m_{\tilde{q}}$  limit. By isolating this scale independent correction we were able to discuss its importance separately.

For sufficiently heavy squarks, it behooves one to introduce the renormalization scale independent effective electron-sneutrino-wino coupling  $\bar{g}_{e\nu\tilde{W}}$ . All corrections proportional to  $\log m_q$  can then be included in the “effective tree level” amplitude, which is obtained by replacing the couplings and mixing matrices of the tree level amplitude  $g_{e\nu\tilde{W}}$ ,  $U$ ,  $V$ , and  $s$ -channel gauge coupling  $g_i$ , with the effective ones  $\bar{g}_{e\nu\tilde{W}}$ ,  $U^P$ ,  $V^P$ , and  $g_i^{\text{SM}}$  respectively. The corrections proportional to  $\log m_{\tilde{q}}$  are included in the first three effective parameters, while  $g_i^{\text{SM}}$  is  $m_{\tilde{q}}$  independent.

Since we only include quark and squark loop corrections, only the external chargino lines receive wave function renormalization, and we discussed the convenience of the introduction of the on-shell effective chargino mixing matrices in that context. We note, however, that our formulation of the effective mixing matrices can be easily extended to the gauge-Higgs loops, and to the wave function renormalization of other external particles with flavor mixing, such as neutralinos.

For gaugino-like charginos, the  $\log m_{\tilde{q}}$  dependence of  $\bar{g}_{e\nu\tilde{W}}$  gives the dominant correction to the production amplitude. The amplitude in Higgsino-like chargino production does not receive corrections proportional to  $\log m_{\tilde{q}}$ . Instead it receives finite corrections from the gauge-Higgsino-Higgsino vertex correction. The correction is rather small even though Yukawa couplings are involved. Numerically we found the correction is of order a few percent. Our numerical calculation is in contradiction with previous results given in Ref. [15]. They claim large corrections to the production cross section of Higgsino-like charginos. We found in some cases order of magnitude

differences with their results. Finally, in mixed chargino production, the corrections to the off-diagonal elements of the effective chargino mass matrix are important, because  $U^P$  and  $V^P$  are sensitive to them. The off-diagonal elements receive corrections proportional to  $\log m_{\tilde{q}}$ , and they also receive decoupling corrections due to squark left-right mixing. Both corrections can be as large as 10%. In order to successfully extract the most useful information from the chargino measurements, it may be necessary to isolate the light top squark mixing effects, for example by measuring the top squark masses and mixing angle through its direct production. Precise measurements of the chargino and neutralino spectrum could also give information on top squark mixing.

The validity of various approximations to the one-loop cross section was also studied in this paper. A simple approximation which works in a wide region of parameter space makes it easy to simulate the effect of the radiative correction in MC studies. We found the 1PI vertex correction may be safely neglected, and we further defined approximations to the rest of the one-loop amplitude. The one-loop cross section is well described by the effective coupling and mixing matrices. These parameters encode the leading  $\log(M_{\tilde{Q}})$  and constant corrections, as well as important decoupling corrections. If these decoupling corrections are dropped, we found that the resulting approximation can be poor even for relatively heavy squark masses,  $m_{\tilde{q}} \sim 1.5\sqrt{s}$ .

Chargino production suffers from  $W$ -boson pair production background at  $e^+e^-$  colliders. Therefore, the detectability of the radiative effect must be studied carefully. Previously studies proceeded by choosing a point in MSSM parameter space, and generating the MC signals utilizing the cuts that reduce the  $WW$  backgrounds while keeping signal events. These cuts were determined in a generic situation in Ref. [6]. In Sec. 4, we pointed out that the point of parameter space chosen in the MC study of Ref. [11] is not consistent with the assumptions used to determine the cuts in Ref. [6]. Namely, at the parameter point of Ref. [11] there is very little phase space in the chargino decay  $\tilde{\chi}_1^- \rightarrow W\tilde{\chi}_1^0$ . As a result, the  $\cancel{p}_T$  distribution of the signal events is similar to that of the background. However, the cuts to reduce the background were chosen under the assumption that the signal would have a higher  $\cancel{p}_T$  distribution relative to the background. We found this causes the very small acceptance. In this situation small changes in the  $\tilde{\chi}_1^-$  and  $\tilde{\chi}_1^0$  masses lead to large variations in the accepted number of events. The expected experimental chargino and neutralino mass error therefore leads to a large systematic error in the chargino production cross section. We suggest the uncertainty at such a point can be reduced by optimizing cuts and beam energy to increase the acceptance. We showed that at generic points in parameter space the acceptance is substantially larger, and the systematic errors due to the chargino and neutralino mass uncertainties will not pose a serious problem. We stress that efforts to optimize cuts to obtain the maximal acceptance greatly reduce the error in the cross section both by increasing statistics and reducing systematic errors. This improves the sensitivity of the measurement to the loop effects.

We note the systematic error due to the theoretical underlying parameters may be reduced by measuring various kinematical distributions of decay products in  $\cancel{p}_T$ ,  $\theta_{\text{acop}}$ , etc. Such fitting to decay distributions has not been considered in previous studies. Furthermore, the decoupling correction is not negligible in the mixed case, and this might introduce an interesting twist in future chargino studies. This will be studied elsewhere. We did not present our fits of chargino production cross section to MSSM parameters. Notice, however, that fits of MC data to MSSM

parameters are sensitive to the specific choice of the theoretical input parameters, beam conditions, etc., chosen for the study. The fitted results at one or a few points in parameter space should not be interpreted generically.

The corrections encoded in  $\bar{g}_{e\tilde{\nu}\tilde{W}}$ ,  $U^P$  and  $V^P$  are universal. They appear in various production and decay processes, and may be important when chargino decay distributions or branching ratios are used in a fit. Neutralino pair production receives analogous  $\log m_{\tilde{q}}$  corrections. Of course the chargino and neutralino corrections are equally important in final states which receive contributions from both chargino and neutralino production.

Previously, information on particles which were not produced directly was ascertained by calculating the effects of loop corrections in SM processes and comparing the predictions with experimental data. Unfortunately, superpartners typically give very small corrections in SM processes because of their decoupling nature. Once a superpartner is found, the existence of heavier superpartners with mass  $M$  gives rise to interesting non-decoupling effects proportional to  $\log M$  in the production and decay processes of the lighter sparticle. In this paper we studied a chargino production process, and compared the  $\log m_{\tilde{q}}$  correction and the associated decoupling corrections in detail. We found the mixing of light third generation squarks also leads important radiative corrections. If these two effects can be separated, we could uncover rich information about the squark mass spectrum. We stress that a systematic treatment of the loop correction and a detailed examination of future experimental prospects are needed to make such a study possible.

## Acknowledgements

We greatly benefitted from discussions with K. Fujii and appreciate the support of the JLC group. We thank Ken-ichi Hikasa for bringing his unpublished note [20] to our attention. M.M.N. thanks the SLAC theory group for generous hospitality. S.K. would like to thank Y. Okada for helpful discussions. M.M.N. is supported in part by Grant in aid for Science and Culture of Japan (07640428, 09246232). D.M.P. is supported by Department of Energy contract DE-AC03-76SF00515.

## Appendix A: Tree level interactions

We list the tree level interactions of charginos, quarks, and squarks. The chargino ( $\tilde{\chi}^-$ ) mass matrix in the gauge eigenbasis,

$$\psi_{iL}^- = (\tilde{W}_L^-, \tilde{H}_{1L}^-), \quad \psi_{iR}^- = (\tilde{W}_R^-, \tilde{H}_{2R}^-), \quad (\text{A.1})$$

is given as [25]

$$-\mathcal{L}_m = \overline{\psi_{iR}^-} M_{Cij} \psi_{jL}^- + \overline{\psi_{iL}^-} M_{Cij}^\dagger \psi_{jR}^-,$$

$$M_C = \begin{pmatrix} M_2 & \sqrt{2}M_W \cos \beta \\ \sqrt{2}M_W \sin \beta & \mu \end{pmatrix}. \quad (\text{A.2})$$

The mass matrix  $M_C$  is diagonalized by two unitary matrices  $V$  and  $U$  as  $M_D = V^* M_C U^\dagger$ , where  $M_D = \text{diag}(m_i)$ . Note that at the one-loop level  $M_W$  in Eq. (A.2) is the  $\overline{\text{DR}}$  renormalized parameter.

The chargino-fermion-sfermion couplings are written as follows:

$$\begin{aligned} \mathcal{L}_{\text{int}} = & -\tilde{f}_{1i}^* \overline{\tilde{\chi}_j^-} \left( a_{\tilde{f}_{1ij}}^- P_L + b_{\tilde{f}_{1ij}}^- P_R \right) f_2 + (\text{h.c.}) \\ & -\tilde{f}_{2i}^* \overline{\tilde{\chi}_j^\mp} \left( a_{\tilde{f}_{2ij}}^+ P_L + b_{\tilde{f}_{2ij}}^+ P_R \right) f_1 + (\text{h.c.}) , \end{aligned} \quad (\text{A.3})$$

where  $f = (q, l)$  and  $(f_1, f_2)$  are SU(2) doublets, and the suffix  $i$  of sfermions denote its mass eigenstates. Explicit forms of  $(a, b)$  in the gauge eigenbasis of sfermions  $\tilde{f}_{L,R}$  are written in terms of  $(U, V)$ , the gauge coupling  $g_2$  and Yukawa couplings  $y_f$  of fermions  $f$  as

$$\begin{aligned} a_{\tilde{f}_{1Li}}^- &= g_2 V_{i1}^* , \quad a_{\tilde{f}_{2Li}}^+ = g_2 U_{i1}^* , \\ a_{\tilde{f}_{1Ri}}^- &= -y_{f1} V_{i2}^* , \quad a_{\tilde{f}_{2Ri}}^+ = -y_{f2} U_{i2}^* , \\ b_{\tilde{f}_{1Li}}^- &= -y_{f2} U_{i2} , \quad b_{\tilde{f}_{2Li}}^+ = -y_{f1} V_{i2} , \\ b_{\tilde{f}_{Ri}}^\mp &= 0 , \end{aligned} \quad (\text{A.4})$$

where

$$y_{f1} = \frac{g_2 m_{f1}}{\sqrt{2} M_W \sin \beta} , \quad y_{f2} = \frac{g_2 m_{f2}}{\sqrt{2} M_W \cos \beta} . \quad (\text{A.5})$$

The gauge interactions of fermions, charginos, and sfermions are expressed as

$$\begin{aligned} \mathcal{L}_{\text{int}} = & -\overline{\tilde{\chi}_i^-} \gamma_\mu \left( v_{Lij}^G P_L + v_{Rij}^G P_R \right) \tilde{\chi}_j^- G^\mu \\ & -\bar{f} \gamma_\mu \left( v_{fL}^G P_L + v_{fR}^G P_R \right) f G^\mu \\ & -i v_{ij}^{\tilde{f}G} \left( \tilde{f}_i^* \overleftrightarrow{\partial}_\mu \tilde{f}_j \right) G^\mu . \end{aligned} \quad (\text{A.6})$$

Here  $G = (\gamma, Z)$  and

$$\begin{aligned} v_{Lij}^G &= (UT^G U^\dagger)_{ij} , \quad v_{Rij}^G = (V^* T^G V^T)_{ij} , \\ T^\gamma &= e \begin{pmatrix} -1 & 0 \\ 0 & -1 \end{pmatrix} , \quad T^Z = g_Z \begin{pmatrix} -1 + \sin^2 \theta_W & 0 \\ 0 & -\frac{1}{2} + \sin^2 \theta_W \end{pmatrix} , \\ v_{fL}^Z &= g_Z (T_{3fL} - Q_f \sin^2 \theta_W) , \quad v_{fR}^Z = -g_Z Q_f \sin^2 \theta_W , \\ v_{LL}^{\tilde{f}Z} &= v_{fL}^Z , \quad v_{RR}^{\tilde{f}Z} = v_{fR}^Z , \quad v_{LR}^{\tilde{f}Z} = v_{RL}^{\tilde{f}Z} = 0 , \\ v_{fL}^{\tilde{f}\gamma} &= v_{fR}^{\tilde{f}\gamma} = e Q_f , \quad v_{ij}^{\tilde{f}\gamma} = e Q_f \delta_{ij} . \end{aligned} \quad (\text{A.7})$$

The mixing of left- and right-handed sfermions may not be negligible for third generation sfermions. The mass matrices for  $\tilde{f} = (\tilde{t}, \tilde{b})$  are given as follows

$$\begin{aligned} -\mathcal{L}_m &= \begin{pmatrix} \tilde{f}_L^* & \tilde{f}_R^* \end{pmatrix} \begin{pmatrix} m_L^2 & m_{LR}^2 \\ m_{LR}^2 & m_R^2 \end{pmatrix} \begin{pmatrix} \tilde{f}_L \\ \tilde{f}_R \end{pmatrix} , \\ m_L^2 &= \tilde{m}_{Q_{3L}}^2 + m_f^2 + m_Z^2 \cos 2\beta (T_{3fL} - Q_f \sin^2 \theta_W) , \\ m_R^2 &= \tilde{m}_{\tilde{f}_{3R}}^2 + m_f^2 + m_Z^2 Q_f \cos 2\beta \sin^2 \theta_W , \\ m_{LR}^2 &= \begin{cases} -m_t (A_t + \mu \cot \beta) & \text{for } \tilde{t} \\ -m_b (A_b + \mu \tan \beta) & \text{for } \tilde{b} . \end{cases} \end{aligned} \quad (\text{A.8})$$

The mass eigenstates  $\tilde{f}_{1,2}$  are obtained by diagonalizing the mass matrices. This leads to the field rotations

$$\begin{aligned}\tilde{f}_1 &= \tilde{f}_L \cos \theta_{\tilde{f}} + \tilde{f}_R \sin \theta_{\tilde{f}} , \\ \tilde{f}_2 &= -\tilde{f}_L \sin \theta_{\tilde{f}} + \tilde{f}_R \cos \theta_{\tilde{f}} ,\end{aligned}\tag{A.9}$$

where  $m_{\tilde{f}_1} < m_{\tilde{f}_2}$ .  $\theta_{\tilde{f}}$  is the mixing angle. Couplings of  $\tilde{f}_{1,2}$  are easily obtained from those in the  $\tilde{f}_{L,R}$  basis.

## Appendix B: Quark and squark loop functions

We list the explicit forms of the quark-squark loop functions in the corrected amplitude shown in Sec. 2. The results are for quarks and squarks of a given generation.

The forms of the chargino two-point functions  $\Sigma_{ij}(p^2)$  are [26]

$$\begin{aligned}\Sigma_{ij}^L(p^2) &= \frac{N_c}{16\pi^2} (a_{\tilde{d}ki}^{+*} a_{\tilde{d}kj}^+ B_1(p^2, m_u, m_{\tilde{d}_k}) + b_{\tilde{u}ki}^- b_{\tilde{u}kj}^{-*} B_1(p^2, m_d, m_{\tilde{u}_k})) , \\ \Sigma_{ij}^R(p^2) &= \frac{N_c}{16\pi^2} (b_{\tilde{d}ki}^{+*} b_{\tilde{d}kj}^+ B_1(p^2, m_u, m_{\tilde{d}_k}) + a_{\tilde{u}ki}^- a_{\tilde{u}kj}^{-*} B_1(p^2, m_d, m_{\tilde{u}_k})) , \\ \Sigma_{ij}^D(p^2) &= \frac{N_c}{16\pi^2} (b_{\tilde{d}ki}^{+*} a_{\tilde{d}kj}^+ m_u B_0(p^2, m_u, m_{\tilde{d}_k}) + a_{\tilde{u}ki}^- b_{\tilde{u}kj}^{-*} m_d B_0(p^2, m_d, m_{\tilde{u}_k})) .\end{aligned}\tag{B.1}$$

Here  $B_{0,1}$  are 't Hooft-Veltman functions in the convention of Ref. [17], and  $N_c = 3$  is color factor.

The one-particle-irreducible (1PI) corrections to the  $\tilde{\chi}_i^+ \tilde{\chi}_j^- G^\mu$  vertices,  $F_V^G$  and  $F_S^G$ , appear in Eq. (6)<sup>||</sup>. The corrections have two parts: contributions from  $(f, f, \tilde{f}'_X)$ -loops (denoted with  $f$ ) and those from  $(f, \tilde{f}'_X, \tilde{f}'_Y)$ -loops (denoted with  $\tilde{f}'$ ), where  $(f, f')$  denotes an SU(2) multiplet of quarks. Accordingly, the  $F^G$ 's are decomposed as

$$\begin{aligned}F_{VL(R)}^G &= \sum_f F_{VL(R)}^{Gf} + \sum_{\tilde{f}} F_{VL(R)}^{G\tilde{f}} , \\ F_{SL(R)}^G &= \sum_f F_{SL(R)}^{Gf} + \sum_{\tilde{f}} F_{SL(R)}^{G\tilde{f}} .\end{aligned}\tag{B.2}$$

The contribution of the  $(f, f, \tilde{f}'_X)$ -loops for  $(f, \tilde{f}') = (d, \tilde{u})$  are expressed as

$$\begin{aligned}F_{VL}^{Gf} &= \frac{N_c}{16\pi^2} \sum_{X=1,2} \left[ b_{X_i} v_R b_{X_j}^* F^{fX} + a_{X_i} v_L a_{X_j}^* m_i m_j (C_{12}^{fX} - C_{11}^{fX}) \right. \\ &\quad + m_f \left\{ -a_{X_i} v_R b_{X_j}^* m_i C_{12}^{fX} - b_{X_i} v_L a_{X_j}^* m_j C_{11}^{fX} \right. \\ &\quad \left. \left. + a_{X_i} v_L b_{X_j}^* m_i (C_0^{fX} + C_{12}^{fX}) + b_{X_i} v_R a_{X_j}^* m_j (C_0^{fX} + C_{11}^{fX}) \right\} \right. \\ &\quad \left. + m_f^2 b_{X_i} v_L b_{X_j}^* C_0^{fX} \right] ,\end{aligned}\tag{B.3}$$

---

<sup>||</sup>There we have ignored additional terms proportional to  $(p_3 + p_4)^\mu$  since their contribution vanishes in the massless electron limit. However, these terms can contribute to other processes such as chargino decays.

$$\begin{aligned}
F_{SL}^{Gf} &= \frac{N_c}{16\pi^2} \sum_{X=1,2} \left[ b_{Xi} v_R b_{Xj}^* m_i (C_{22}^{fX} - C_{23}^{fX}) \right. \\
&\quad + a_{Xi} v_L a_{Xj}^* m_j (C_{11}^{fX} - C_{12}^{fX} + C_{21}^{fX} - C_{23}^{fX}) \\
&\quad \left. + m_f \left\{ a_{Xi} v_R b_{Xj}^* C_{12}^{fX} - a_{Xi} v_L b_{Xj}^* (C_0^{fX} + C_{11}^{fX}) \right\} \right]. \tag{B.4}
\end{aligned}$$

Here we abbreviate  $a_{Xi} = a_{\tilde{f}'Xi}^-$ ,  $b_{Xi} = b_{\tilde{f}'Xi}^-$ , and  $v_{L(R)} = v_{f,L(R)}^G$ . The  $F_R^{Gf}$  formula are obtained from the corresponding  $F_L^{Gf}$  expressions by replacing  $a_{Xi} \leftrightarrow b_{Xi}$  and  $v_L \leftrightarrow v_R$ .  $C_0^{fX}$  and  $C_{\alpha\beta}^{fX}$  are the Passarino and Veltman [27]  $C$  functions in the convention of [28]. The arguments of the  $C$  function are

$$C_{0(\alpha\beta)}^{fX} = C_{0(\alpha\beta)}(p_j^2, p_i^2, s, m_f^2, m_{\tilde{f}'X}^2, m_f^2). \tag{B.5}$$

The function  $F^{fX}$  is defined as

$$F^{fX} \equiv -\frac{1}{2} \left\{ B^{fX} - s C_0^{fX} + (m_{\tilde{f}'X}^2 - m_f^2 + m_i^2 - s) C_{11}^{fX} + (m_f^2 - m_{\tilde{f}'X}^2 - m_i^2) C_{12}^{fX} - 1 \right\}, \tag{B.6}$$

where  $B^{fX} = B_0(p_j^2, m_f^2, m_{\tilde{f}'X}^2)$ .

The contributions of  $(f, \tilde{f}'_X, \tilde{f}'_Y)$ -loops for  $(f, \tilde{f}') = (d, \tilde{u})$  are expressed as follows

$$F_{VL}^{G\tilde{f}'} = \frac{N_c}{16\pi^2} \sum_{XY} 2b_{Xi} v_{XY} b_{Yj}^* C_{24}^{\tilde{f}'XY}, \tag{B.7}$$

$$\begin{aligned}
F_{SL}^{G\tilde{f}'} &= -\frac{N_c}{16\pi^2} \sum_{XY} \left[ m_f a_{Xi} v_{XY} b_{Yj}^* (C_{12}^{\tilde{f}'XY} - C_{11}^{\tilde{f}'XY}) + m_i b_{Xi} v_{XY} b_{Yj}^* (C_{23}^{\tilde{f}'XY} - C_{22}^{\tilde{f}'XY}) \right. \\
&\quad \left. + m_j a_{Xi} v_{XY} a_{Yj}^* (C_{23}^{\tilde{f}'XY} - C_{21}^{\tilde{f}'XY} + C_{12}^{\tilde{f}'XY} - C_{11}^{\tilde{f}'XY}) \right]. \tag{B.8}
\end{aligned}$$

The  $F_R^{G\tilde{f}'}$  are obtained from Eqs. (B.7–B.8) by replacing  $a_{Xi} \leftrightarrow b_{Xi}$ . Here,  $v_{XY} = v_{XY}^{\tilde{f}'G}$ , and

$$C_{0(\alpha\beta)}^{\tilde{f}'XY} = C_{0(\alpha\beta)}(p_j^2, p_i^2, s, m_{\tilde{f}'Y}^2, m_f^2, m_{\tilde{f}'X}^2). \tag{B.9}$$

The contributions for  $(f, \tilde{f}') = (u, \tilde{d})$  loops can be obtained from the  $(f, \tilde{f}') = (d, \tilde{u})$  expressions in Eqs. (B.3–B.4, B.7–B.8) by replacing  $a_{\tilde{f}'Xi}^- \rightarrow b_{\tilde{f}'Xi}^{+*}$ ,  $b_{\tilde{f}'Xi}^- \rightarrow a_{\tilde{f}'Xi}^{+*}$ ,  $v_{f,L}^G \leftrightarrow -v_{f,R}^G$ , and  $v_{XY}^{\tilde{f}'G} \rightarrow -v_{XY}^{\tilde{f}'G}$ .

## Appendix C: Helicity amplitude method

In the calculation of cross sections it is often useful to directly evaluate the amplitude for helicity eigenstates of initial and final state particles, and numerically take the sum of the squared amplitudes for helicities, instead of taking the trace of the squared amplitude analytically. This method is called the helicity amplitude method [19, 20].

In this appendix we list the spinor bilinears which are relevant in the one-loop amplitude of the process  $e^-(p_1, h_1)e^+(p_2, h_2) \rightarrow \tilde{\chi}_i^-(p_3, h_3)\tilde{\chi}_j^+(p_4, h_4)$ .  $h_{1-4}$  are the helicities of the corresponding particles and take the values  $\pm 1/2$ . We evaluate the spinor bilinears in the center of mass frame.

The coordinate space is chosen so that the initial  $e^-$  goes along the positive  $z$  axis and the final  $\tilde{\chi}_i^-$  goes along the  $(\theta, \phi)$  direction in the polar basis. We give our results in the spherical basis. A Lorentz vector in the spherical basis,  $(A^\diamond, A^m)$  with  $m = 0, \pm$ , is related to the vector  $A^\mu$  in the Minkowski basis via

$$\begin{aligned} A^\diamond &= A^0, \\ A^+ &= -\frac{1}{\sqrt{2}}(A^1 + iA^2), \\ A^0 &= A^3, \\ A^- &= \frac{1}{\sqrt{2}}(A^1 - iA^2). \end{aligned} \tag{C.1}$$

The inner product of two vectors  $(A, B)$  is given by

$$A \cdot B \equiv A^\diamond B^\diamond + \sum_m (-1)^{m+1} A^m B^{-m}. \tag{C.2}$$

The initial massless fermion bilinears  $H$  (we ignore the electron mass) and final fermion bilinears  $\bar{H}$  are given in the spherical basis as

$$\begin{aligned} H_V^\mu &\equiv \bar{v}_{h_2}(p_2)\gamma^\mu u_{h_1}(p_1) = \left(0, 2\sqrt{2}|\lambda_I|E\delta_{-m,\lambda_I}\right), \\ H_A^\mu &\equiv \bar{v}_{h_2}\gamma^\mu\gamma_5 u_{h_1} = (-1)^{h_2+1/2} H_V^\mu, \\ \bar{H}_S &\equiv \bar{u}_{h_3}(p_3)v_{h_4}(p_4) = \left((E_3 + E_4)^2 - (m_i + m_j)^2\right)^{1/2} \delta_{\lambda_F 0}, \\ \bar{H}_P &\equiv \bar{u}_{h_3}\gamma_5 v_{h_4} = (-1)^{h_4+1/2} \left((E_3 + E_4)^2 - (m_i - m_j)^2\right)^{1/2} \delta_{\lambda_F 0}, \\ \bar{H}_V^\mu &\equiv \bar{u}_{h_3}\gamma^\mu v_{h_4} = \left(\left[\sqrt{E_3 + m_i}\sqrt{E_4 - m_j} - \sqrt{E_3 - m_i}\sqrt{E_4 + m_j}\right] \delta_{\lambda_F 0}, \right. \\ &\quad \left. -(\sqrt{2})^{|\lambda_F|} \sqrt{\frac{E_3 + m_i}{E_4 + m_j}} \left[E_4 + m_j - (-1)^{\lambda_F}(E_3 - m_i)\right] d_{m\lambda_F}^1(\theta) e^{i(m-\lambda_F)\phi}\right), \\ \bar{H}_A^\mu &\equiv \bar{u}_{h_3}\gamma^\mu\gamma_5 v_{h_4} = (-1)^{h_4+1/2} \left(\sqrt{\frac{E_4 + m_j}{E_3 + m_i}} \left[-E_4 + E_3 + m_i + m_j\right] \delta_{\lambda_F 0}, \right. \\ &\quad \left. -(\sqrt{2})^{|\lambda_F|} \left[(-1)^{\lambda_F+1} \sqrt{E_3 - m_i}\sqrt{E_4 + m_j} + \sqrt{E_3 + m_i}\sqrt{E_4 - m_j}\right] d_{m\lambda_F}^1(\theta) e^{i(m-\lambda_F)\phi}\right). \end{aligned} \tag{C.3}$$

We use the abbreviations  $\lambda_I \equiv h_1 - h_2$  and  $\lambda_F \equiv h_3 - h_4$ .  $(E, E_3, E_4)$  are the  $(e^-, \tilde{\chi}_i^-, \tilde{\chi}_j^+)$  energies, respectively. The relevant Wigner  $d$ -functions  $d_{m\lambda}^1(\theta)$  are

$$\begin{pmatrix} d_{++}^1 & d_{+0}^1 & d_{+-}^1 \\ d_{0+}^1 & d_{00}^1 & d_{0-}^1 \\ d_{-+}^1 & d_{-0}^1 & d_{--}^1 \end{pmatrix}(\theta) = \begin{pmatrix} \frac{1+\cos\theta}{2} & -\frac{1}{\sqrt{2}}\sin\theta & \frac{1-\cos\theta}{2} \\ \frac{1}{\sqrt{2}}\sin\theta & \cos\theta & -\frac{1}{\sqrt{2}}\sin\theta \\ \frac{1-\cos\theta}{2} & \frac{1}{\sqrt{2}}\sin\theta & \frac{1+\cos\theta}{2} \end{pmatrix}. \tag{C.4}$$

## References

- [1] S. Dimopoulos, S. Raby, F. Wilczek, Phys. Rev. D **24**, 1681 (1981); L.E. Ibáñez, G.G. Ross, Phys. Lett. **B105**, 439 (1981); U. Amaldi *et al.*, Phys. Rev. D **36**, 1385 (1987); J. Ellis, S. Kelley, D.V. Nanopoulos, Phys. Lett. **249B**, 441 (1990); P. Langacker, M.-X. Luo, Phys. Rev. D **44**, 817 (1991); U. Amaldi, W. de Boer, H. Fürstenau, Phys. Lett. **260B**, 447 (1991); P. Langacker, N. Polonsky, Phys. Rev. D **47**, 4028 (1993); *ibid.* D **52**, 3081 (1995); P.H. Chankowski, Z. Pluciennik, S. Pokorski, Nucl. Phys. **B349**, 23 (1995); J. Bagger, K. Matchev, D. Pierce, Phys. Lett. **348B**, 443 (1995).
- [2] The LEP collaborations ALEPH, DELPHI, L3, OPAL, the LEP Electroweak Working Group and the SLD Heavy Flavour Group, preprint CERN-PPE/96-183; Particle Data Group, R.M. Barnett *et al.*, Phys. Rev. D **54**, 1 (1996) and off-year update URL <http://pdg.lbl.gov>.
- [3] I. Hinchliffe, F.E. Paige, M.D. Shapiro, J. Soderqvist, W. Yao, Phys. Rev. D **55**, 5520 (1997).
- [4] D.G. Cassel, L. Trindle Gennari, R.H. Siemann (eds.), “New direction for High Energy Physics”, proceedings of the 1996 DPF/DPB Summer Study on High-Energy Physics, June 25-July 12, 1996, Snowmass, Colorado.
- [5] JLC Group, JLC-1, KEK Report No. 92–16 (1992).
- [6] T. Tsukamoto *et al.*, Phys. Rev. D **51**, 3153 (1995).
- [7] J.L. Feng, M.E. Peskin, H. Murayama, X. Tata, Phys. Rev. D **52**, 1418 (1995).
- [8] M.M. Nojiri, K. Fujii, T. Tsukamoto, Phys. Rev. D **54**, 6756 (1996).
- [9] P.H. Chankowski, Phys. Rev. D **41**, 2877 (1990).
- [10] K. Hikasa, Y. Nakamura, Z. Phys. C **70**, 139 (1996); **71**, 356(E) (1996).
- [11] H.-C. Cheng, J.L. Feng, N. Polonsky, Phys. Rev. D **56**, 6875 (1997); **57**, 152 (1998).
- [12] L. Randall, E. Katz, S. Su, hep-ph/9706478; hep-ph/9801416.
- [13] M.M. Nojiri, D.M. Pierce, Y. Yamada, Phys. Rev. D **57**, 1539 (1998).
- [14] W. Siegel, Phys. Lett. **84B**, 193 (1979); D.M. Capper, D.R.T. Jones, P. van Nieuwenhuizen, Nucl. Phys. **B167**, 479 (1980); I. Antoniadis, C. Kounnas, K. Tamvakis, Phys. Lett. **119B**, 377 (1982).
- [15] M.A. Díaz, S.F. King, D.A. Ross, hep-ph/9711307.
- [16] J.A. Grifols, J. Solà, Nucl. Phys. **B253**, 47 (1985).
- [17] D.M. Pierce, J.A. Bagger, K.T. Matchev, R.-J. Zhang, Nucl. Phys. **B491**, 3 (1997).
- [18] K.-I. Aoki, Z. Hioki, R. Kawabe, M. Konuma, T. Muta, Prog. Theor. Phys. Suppl. **73**, 1 (1982); M. Böhm, H. Spiesberger, W. Hollik, Fortschr. Phys. **34**, 687 (1986).



- [19] M. Jacob, G.C. Wick, *Ann. Phys.* **7**, 404 (1959); H.E. Haber, “Spin formalism and applications to new physics search”, hep-ph/9405376, in *Stanford 1993, Spin structure in high energy processes* (ed. L. Deporcel and C. Dunwoodie), 231-272, SLAC-Report-444 (1994).
- [20] K. Hikasa, unpublished.
- [21] A. Denner, T. Sack, *Nucl. Phys.* **B347**, 203 (1990); B.A. Kniehl, A. Pilaftsis, *Nucl. Phys.* **B474**, 286 (1996).
- [22] M. Drees, K. Hikasa, *Phys. Lett.* **252B**, 127 (1990)
- [23] V. Barger, M.S. Berger, T.Han, hep-ph/9801410.
- [24] H. Baer, R. Munroe, X. Tata, *Phys. Rev. D* **54**, 6735 (1996).
- [25] J.F. Gunion, H.E. Haber, *Nucl. Phys.* **B272**, 1 (1986); **B402**, 567(E) (1993).
- [26] D. Pierce, A. Papadopoulos, *Nucl. Phys.* **B430**, 278 (1994); *Phys. Rev. D* **50**, 565 (1995).
- [27] G. Passarino, M. Veltman, *Nucl. Phys.* **B160**, 151 (1979).
- [28] K. Hagiwara, D. Haidt, C.S. Kim, S. Matsumoto, *Z. Phys. C* **64**, 559 (1994); **68**, 352(E) (1995).